

Review

Pseudocapacitive Storage in High-Performance Flexible Batteries and Supercapacitors

Zhenxiao Lu ^{1,*}  and Xiaochuan Ren ² 

¹ School of Chemical and Pharmaceutical Engineering, Nanyang Normal University, Nanyang 473061, China

² Institute of Materials for Energy and Environment, Qingdao University, Qingdao 266071, China;
rxchuan@qdu.edu.cn

* Correspondence: 20212001@nynu.edu.cn

Abstract: Attention to electrochemical energy storage (EES) devices continues to grow as the demand increases for energy storage systems in the storage and transmission of renewable energy. The expanded market requirement for mobile electronics devices and flexible electronic devices also calls for efficient energy suppliers. EES devices applying pseudocapacitive materials and generated pseudocapacitive storage are gaining increasing focus because they are capable of overcoming the capacity limitations of electrical double-layer capacitors (EDLCs) and offsetting the rate performance of batteries. The pseudocapacitive storage mechanism generally occurs on the surface or near the surface of the electrode materials, which could avoid the slow ion diffusion process. Developing materials with beneficial nanostructures and optimized phases supporting pseudocapacitive storage would efficiently improve the energy density and charging rate for EES devices, such as batteries and flexible supercapacitors. This review offers a detailed assessment of pseudocapacitance, including classification, working mechanisms, analysis methods, promotion routes and advanced applications. The future challenges facing the effective utilization of pseudocapacitive mechanisms in upcoming energy storage devices are also discussed.

Keywords: energy storage; pseudocapacitive storage; batteries; flexible supercapacitors; pseudocapacitance; analysis methods; advanced application



Academic Editor: Ottorino Veneri

Received: 3 January 2025

Revised: 30 January 2025

Accepted: 5 February 2025

Published: 7 February 2025

Citation: Lu, Z.; Ren, X.

Pseudocapacitive Storage in High-Performance Flexible Batteries and Supercapacitors. *Batteries* **2025**, *11*, 63.

<https://doi.org/10.3390/batteries11020063>

Copyright: © 2025 by the authors.

Licensee MDPI, Basel, Switzerland.

This article is an open access article distributed under the terms and conditions of the Creative Commons Attribution (CC BY) license (<https://creativecommons.org/licenses/by/4.0/>).

1. Introduction

The era of fossil fuels dominating the energy supply has passed; low-carbon development and low-carbon life are now greatly advocated and strongly supported [1]. Traditional energy is giving way to clean and inexhaustible resources, such as the sun, tides and wind. Thus, it is vital to develop and apply efficient and cost-effective energy storage devices to collect these intermittent resources and export them to stable daily utilization [2–4]. Multi-formity of the applications necessitates the manifoldness of equipment development and technique, leading to the diversity of power accumulators. Electrochemical energy storage (EES) equipment, including batteries and double-layer capacitors (EDLCs), are identified as optional candidates because of their cost-effectiveness and eco-friendliness [5–7]. The energy storage mechanisms of the EES devices are quite different: the charge storage in EDLCs occurs through electrostatic accumulation of various charges at the interface of electrode/electrolyte, while batteries traditionally store energy in the form of electrochemical reactions [8–10]. In EDLCs, the non-faradic process is the main storage mechanism, which takes place over the surface of the electrode material electrostatically and is accompanied by the reversible adsorption of ions. The batteries apply the faradic process, which would be

the conversion reaction happening on the surface of the raw materials, or in the inner space of the raw materials [11–13]. However, both EDLCs and batteries are facing limitations originating from their operating mechanisms. Batteries suffer from poor rate performance and unsatisfactory energy storage due to the sluggish reaction kinetics originating from the low ion diffusion efficiency in the inner space of the electrode materials. Furthermore, safety and reliability are still big tasks that need to be overcome [14–16]. The EDLCs, compared to batteries, possess a shorter charging time and much higher power, but are limited by lower energy density [17].

An EES device employing a pseudocapacitive energy storage mechanism is an intermediate device between capacitors and batteries, which possesses a hybrid storage mechanism and is able to remedy the shortage of the above two devices. In 1962, pseudocapacitance was first reported as an energy accumulator similar to capacitors, proved by the cyclic voltammograms (CV) curves of hydrous RuO₂ films in acidic electrolyte [18]. They confirmed that pseudocapacitance supports fast and reversible electrochemical reactions, exhibiting a high energy storage and rate property compared to EDLCs and batteries [19–21]. In 1999, Lee and Goodenough reported the capacitor-like charge storage in a disordered MnO_x electrode accompanied by a mild-PH electrolyte, which was the predecessor of pseudocapacitors and opened a new route for designing high performance electrochemical devices [22–24]. According to the reports, pseudocapacitive materials store energy based on the faradic process occurring on or near the surface of the electrode materials, which is similar to the storage process in the batteries. However, the pseudocapacitive storage process could supply higher energy in shorter time due to the high reversibility and fast reaction kinetics of the pseudocapacitive behavior [25–29]. The significance of researching pseudocapacitive electrode materials is to overcome the kinetic limitation plaguing LIBs while achieving energy densities higher than those of EDLCs. Developing and applying electrode materials enabling pseudocapacitive storage in batteries or flexible devices may realize high energy and fast charging rates simultaneously [30–34]. Thus, it is foundational and essential to study the mechanisms of the pseudocapacitive storage process, including, electrochemical nature features, energy transformation, ion transportation paths, and reaction patterns.

In this review, the foundational electrochemical theories involve three kinds of EES devices, including diffusion principles of ions, kinetic characteristics, and storage mechanisms, which are summarized. We especially emphasize and concentrate on pseudocapacitive storage. Comprehensive classification of pseudocapacitive storage according to the updated reports are supplied. We summarize the calculation, simulation, and testing methods to identify pseudocapacitance, quantitatively analyze the pseudocapacitive contribution to total storage process, and trace the phase transformation during the storage process. The design strategies and methods to introduce or enlarge the pseudocapacitive effect are discussed. Some advanced applications of pseudocapacitive storage except for the three main EES devices are listed. Finally, future trends in pseudocapacitive storage are briefly discussed.

2. Principles Involved in the Energy Storage Process

2.1. Diffusion Mechanisms

Based on the seven diverse Bravais lattice system, there are three diffusion paths for ions (Li⁺, Na⁺, K⁺, Zn²⁺) in the lattice: interlayer diffusion, vacancy diffusion, gap diffusion, and interstitial diffusion [35]. Typically, interlayer diffusion refers to the process of ion embedding into the crystalline structure of the electrode and accompanied phase transformation, which results in poor rate performance and low charge capacity [36–40]. Vacancy diffusion refers to the ion diffusion process associated with Schottky vacancy diffusion, while gap diffusion is related to the Frank interstitial diffusion process. The

interstitial diffusion mechanism, also called direct diffusion, is applied in the diffusion of interstitial atoms in solid solution, where minute-sized interstitial atoms migrate from one interstitial site to another [35] (Figure 1a).

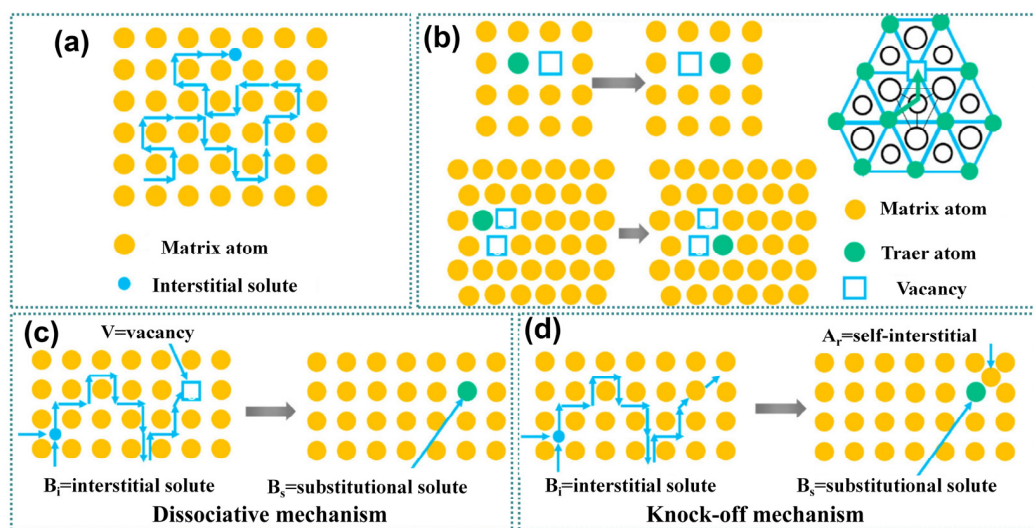


Figure 1. (a) Direct, (b) vacancy, and (c,d) gap-replacement exchange diffusion mechanism [35]. Copyright 2024, American Chemical Society.

The vacancy mechanism is employed in replacement solid solutions, where atoms migrate via leaping to neighboring vacancies (Figure 1b) [41,42]. For replacement solid solutions, a tiny diversity of atomic diameter would hinder the occurrence of interstitial diffusion. The above discussion demonstrates the importance of vacancy diffusion in the solids [35]. Generally, a multi-vacancy mechanism would execute when plenty of vacancies generate via doping in order to increase ionic conductivity. Atoms can diffuse through the interaction of interstitial lattice sites when atoms possess interstitial and lattice sites simultaneously [35]. The interstitial substituent interaction generally generates if the concentration of the interstitial solute atoms is lower than that of the substituent atoms. The dissociative mechanism is used when the diffusion is accomplished through vacancies (Figure 1c). Otherwise, the collective diffusion mechanism would exist, where several atoms migrate in a chain-like or track-like path simultaneously (Figure 1d). Both the knock-off sub-mechanism and the self-gap mechanism are typical collective diffusion mechanisms.

2.2. Energy Storage Mechanisms

The conventional battery-type electrode material features with reversible redox electrochemical reactions dominating the charge storage process, which is perceived to be a faradic process (Figure 2a) [43]. In the charge process: 1. The voltage applied by an external power source produces an electric field inside the battery. In the positive materials (such as lithium cobaltate), Li^+ moves from the crystal structure under the electric field and enters the electrolyte. 2. Li^+ moves in the electrolyte through diffusion and migration. Diffusion is the random thermal movement caused by the concentration gradient, while migration is the directional movement of Li^+ under the electric field. 3. Li^+ is embedded in the anode material. During the embedding process, the crystal structure of the anode material changes, and the charge is redistributed. In the discharge process: 1. Li^+ escapes from the negative electrode. 2. The Li^+ returns to the positive electrode through the electrolyte. This process is the opposite of the charging process, in which Li^+ is re-embedded into the crystal structure of the positive electrode material through the electrolyte. 3. Electrons flow through an external circuit. In this process, electrons flow from the negative electrode back to the positive electrode, providing power to the load. Accordingly, the storage process

is severely influenced by the long ion diffusion distance, dull electrochemical reaction kinetics, and irreversible structural change during ion intercalation/deintercalation. Thus, the obtained capacity is abridged and the rate capability is not satisfied to support the fast-charging equipment for practical application [44]. Compared to the “high-energy” yielded by a battery system, a supercapacitor is regarded as a “high-power system”. To settle down this evident obstacle of batteries, one feasible method is to develop a hybrid charge system that employs both battery-type and capacitive electrochemical processes to gather the high power and high energy simultaneously [45–47].

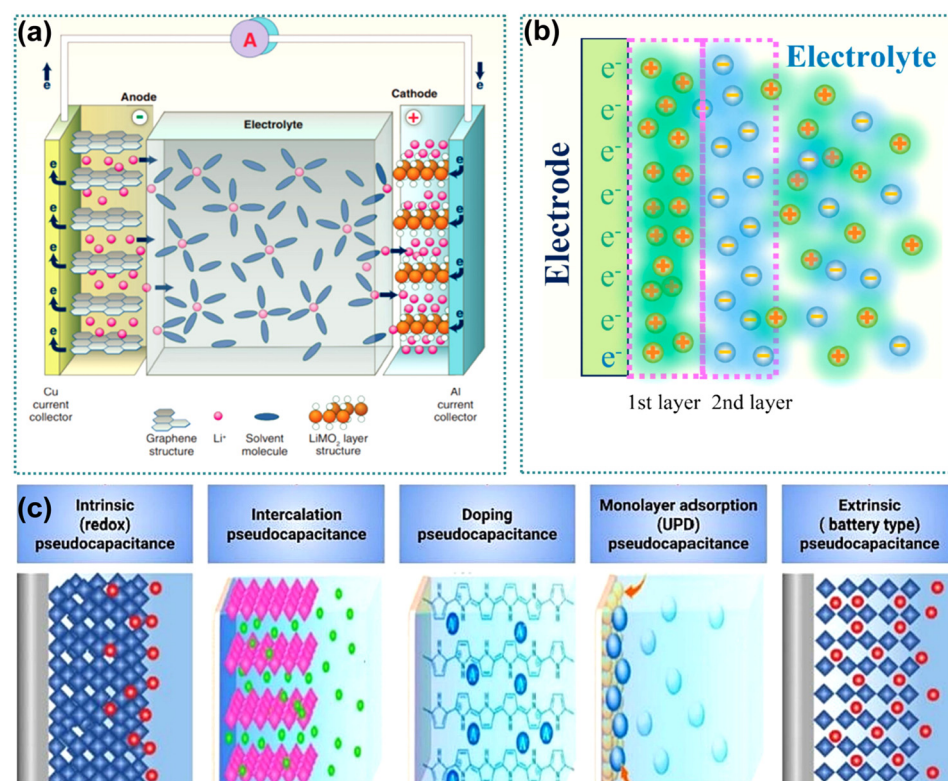


Figure 2. Schematic diagram of (a) Li-ion battery [35,48], and (b) electrochemical reaction in double-layer capacitors [25,35,48]. Copyright 2024, American Chemical Society. (c) Classification of pseudocapacitance mechanism [49]. Copyright 2023, Elsevier.

2.3. Storage Mechanism in Electrical Double-Layer Capacitor (DELc)

The DELC stores energy based on the double-layer structure formed via the adsorption of anions and cations at the interface of the electrode and the electrolyte [50–53] (Figure 2b). The capacitance is closely related to the properties of the connected electrode surface accessible to the ions in the electrolyte. During the charging process, the anions move to the positive electrode and the cations move to the negative electrode material through the electrolyte, while the electrons move to the positive electrode material through an external loop [54,55]. The DELC storage process can be described using the Helmholtz model for the parallel plate capacitor by the following equation:

$$C = \epsilon A/d \quad (1)$$

where C is the capacitance of the double-layer, ϵ is the permittivity of the dielectric separating charges, A is the surface area of the electrode, and d is the distance between the electrode and electrolyte ions [56]. Further, the charging/discharging process of the EDLC belongs to non-Faradic processes, which largely depend on the potential changes. As previously reported, carbon-based porous materials, such as activated carbon [57–59], xerogels [60–63],

carbon nanotubes (CNTs) [64–66], carbon nanofibers (CNFs) [67–69], graphene [70–72], and carbide-derived carbons [73–75] which show typical EDLC behavior due to their high conductivity and high specific surface area. However, these carbon-based EDLCs obtain low energy density, which hinders the practical application.

2.4. Pseudocapacitive Storage Mechanism

The redox reaction in the pseudocapacitance mechanism involves the gain and loss of electrons, and is accompanied by the charge transfer process. In pseudocapacitors, the redox reaction is mainly carried out on the surface of the active material. This is different from the physical energy storage process of capacitors, which does not involve the transfer of electrons [49]. Specifically, when ions in solution are electrochemically adsorbed to the surface or near the surface of the active substance, they undergo a redox reaction and enable the storage of energy. Therefore, pseudocapacitors show unique advantages in energy storage and conversion. In addition, it is worth noting that the redox reaction and charge transfer process of pseudocapacitors may be affected by many factors, such as the type of active material, morphology, particle size, and composition of the electrolyte [76,77].

For the pseudocapacitive electrode, the total storage originates from three parts: 1. the faradic process along with the ion diffusion, 2. the faradic process controlled by the charge transfer reaction of the surface molecule and the atoms at the interstitial interface inside the electrode, and 3. the non-faradic process from the double-layer capacitance. The capacity originating from the second and the third storage mechanism is indivisible and is denoted as a pseudocapacitive contribution to the total storage. Significantly, the pseudocapacitance helps the batteries withstand wider charge voltage while maintaining stable cycling and long lifespan [78]. The pseudocapacitive behavior can obtain high charge capacity at high charge rate without the limitations from solid-state diffusion and produce high power density to compensate for the limited energy density of the battery to some extent [79–81]. This beneficial feature enables pseudocapacitive materials to support batteries possessing fast-charging capacity, favorable energy, and high power density simultaneously.

Up to now, pseudocapacitance could be subdivided into five kinds according to their storage mechanisms (Figure 2c): (1) intrinsic pseudocapacitance or redox pseudocapacitance (as in $\text{RuO}_2 \cdot \text{H}_2\text{O}$), (2) intercalation pseudocapacitance, (3) doping pseudocapacitance, (4) monolayer adsorption (underpotential deposition) pseudocapacitance, (5) extrinsic pseudocapacitive. These lead to different features of electrochemical response and applications. Figure 2c displays the comparison of different pseudocapacitive mechanisms [82–85].

2.4.1. Intrinsic Pseudocapacitance

Intrinsic pseudocapacitive behavior (also known as redox pseudocapacitance or surface redox pseudocapacitance) is independent of the morphological and structural influence of the material. These materials maintain their pseudocapacitive nature based on faradic redox reactions happening on or near the electrode surface, or at the interface of electrode and electrolyte [86,87]. The intrinsic pseudocapacitance manifests efficient reaction kinetics, because the cations are free of the long-range diffusion process and the confrontation with the van der Waals force is avoided [88]. Furthermore, the surface redox pseudocapacitance hardly causes distinct volume/phase changes that can be detected after long-term cycling, which supports the outstanding cycling stability for high-rate energy storage [89]. Typical examples include transition metal oxide and some conductive polymers [90].

2.4.2. Intercalation Pseudocapacitance

Intercalation pseudocapacitance stores energy when the cations embed into the layers of the redox-active electrode material without crystallographic phase transformation [91]. The intercalation pseudocapacitance shows unique high-rate performance which enables

a fairly fast charging rate. Generally, the storage efficiency is hindered by generally slow insertion into the van der Waals gap, and limited solid-state phase transformation and the accompanying extremely small lattice strain [92–94]. However, Conway and his team reported that the insertion could happen efficiently via an intercalation pseudocapacitive process, where the charge was stored without the phase transformation [95]. Intercalation pseudocapacitive storage could occur not only on the surface, but also in the 1D or 2D channels in materials with 1D or 2D microstructure [96,97]. This process prompts the ions to fill in the vacancy defects and tunnels in the bulk material, which results in accelerated charge transfer [98]. Intercalation pseudocapacitive materials, including MoS₂, Co(OH)₂, TiS₂, and T-Nb₂O₅ and transition metal carbides [99,100], display better rate performance and more stable cycling stability compared with battery materials [101,102].

2.4.3. Monolayer Adsorption Pseudocapacitance

Monolayer adsorption (underpotential deposition) pseudocapacitance depends on the process of metal monolayer electro-deposition on another metal substrate under a negative potential above their redox potential. In this mechanism, the charge transfer reaction between the adsorbed metal monolayers and the substrate contribute highly reversible cyclicity corresponding to different adsorbed structures [16,83]. This process associates with the adsorption of protons (H⁺) and lead ions (Pb²⁺) on the surface of precious metal (Ag, Au) at low applied voltage. However, the monolayer adsorption (or underpotential deposition) pseudocapacitance is rarely applied in practical utilization due to the high price and narrow voltage window [16,103].

2.4.4. Doping Pseudocapacitance

Carbon-based electrode materials are reported to possess EDLC storage behavior and capable of achieving the extra advantage of pseudocapacitance through doping different functional groups, which is named as doping pseudocapacitance. The electrochemical response of doping pseudocapacitive electrodes is closely associated with the nature of the doped dopants [104,105]. The relationship between the doped dopants and electrochemical response can be summarized as follows: (1) Heteroatoms doping improves the overall performance of the supercapacitor cell by contributing through pseudo-capacitance and by enhancing ion transfer kinetics (by improving electrode/electrolyte wettability) [104]. (2) Oxygen-containing functional and the heteroatoms (N, P) introduced to the graphene system may lead to deformation in the CV curves when compared with samples without heteroatom doping [105]. (3) Dual-doping always brings a greater pseudocapacitive contribution compared with mono-doping [105–108].

2.4.5. Extrinsic Pseudocapacitance

Notably, the extrinsic pseudocapacitive mechanism is highly tunable and flexible, and determined by the size, morphology, and composition of the electrode. Thus, extrinsic pseudocapacitance is highly practicable and common in energy storage [109–112]. The extrinsic pseudocapacitance is a kind of induced pseudocapacitance, which can be imported to faradic diffusion-controlled process by modifying traditional electrode material based on particular methods, such as size adjustment, compound design, element doping, anion intercalation, and morphological optimization [113]. Extrinsic pseudocapacitance paves an accessible road between the conventional battery-type electrode and the pseudocapacitive electrode, which would contribute to the development of an energy storage technique with hybrid functionality [114–116].

3. Identification and Quantitative Analysis

3.1. Electrochemical Analysis

Pseudocapacitance can be identified and quantitatively calculated by analyzing CV curves at a series of different scan rates. The pseudocapacitive contribution to the high-rate performance of battery-type materials can be quantitatively analyzed by separating the capacitive current from the traditional diffusion-controlled current. In the charging process of a pseudocapacitive material, the total current at a certain potential is composed of the contribution from the capacitance-controlled electric double layer charging which generates fast faradic reactions at the interface of electrolyte and electrode (i_c) and the contribution from the conventional diffusion-controlled process (i_d) [117]. Thus, the current can be expressed as the Equation (2) and the deformation Equation (3).

$$i(v) = i_c + i_d = av^b \quad (2)$$

$$\log i(v) = \log (av^b) = \log (a) + b \log (v) \quad (3)$$

In Equation (3), a and b are symptomatic parameters and correspond to the nature of the reaction kinetics [118,119]. The parameter b equals the slope of the log (peak current) versus log (sweep rate) linear plot (Figure 3a), which reveals the pseudocapacitive mechanisms involved in the reaction. If $b = 1$, the capacitive contribution, which is controlled by the near-surface electrochemical process including pseudocapacitance and EDLC, dominates the storage [26]. For example, the Nb_2O_5 electrode, with “ b ” value close to 1, shows intercalation pseudocapacitance which can be attributed to a surface phenomenon [92]. Nevertheless, the “ b ” value of bulk materials, like LiFePO_4 , is 0.5, indicating the diffusion-controlled faradic reactions (Figure 3a) [119]. That is to say, diffusion-controlled faradic mechanisms tend to decrease the “ b ” value, while the capacitive process contributes to raising the “ b ” value [26]. When the “ b ” value is between 1 and 0.5, corresponding to the green area (named as transition region) in Figure 3a, the electrode would exhibit an intermediate electrochemical feature between battery type and capacitive behaviors [26,118,120,121]. The role of pseudocapacitance and extrinsic pseudocapacitance among the energy storage devices is shown in Figure 3b according to Yu et al. [20]. Pseudocapacitors balance the high energy of batteries and the high power of EDLCs (Figure 3b).

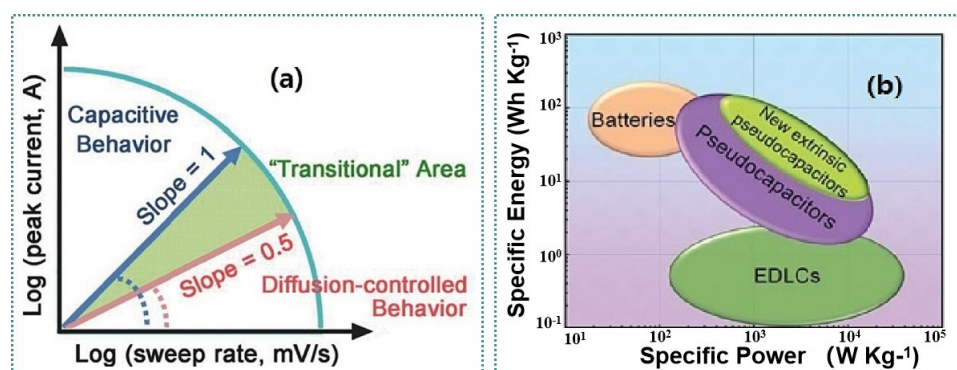


Figure 3. (a) Peak current vs. sweep rate plot showing power law dependence and the variation in nature of capacitive nature with the change in slope value [26,49]. Copyright 2023, Elsevier. (b) Comparison of energy storage performance of EDLCs, batteries, pseudocapacitors, and expected performance of extrinsic pseudocapacitors [20,49]. Copyright 2023, Elsevier.

3.2. X-Ray Analytical Techniques

The reversible redox pseudocapacitive process takes place not only at the surface of the electrode but also in the bulk phase inside the electrode [122]. In order to gain deeper

comprehension about the mechanism and procedure of the pseudocapacitance, more methods and tools are applied to detect the pseudocapacitive behavior. Characterization methods based on X-ray, including XRD, synchrotron XRD, in situ or ex situ XRD, in situ or ex situ X-ray Photoelectron Spectroscopy (XPS), X-ray Absorption Spectroscopy (XAS), X-ray Absorption Fine Spectroscopy (XAFS), X-ray absorption near edge structure (XANES), and Extended XAFS (EXAFS) are always used to reveal the phase transformation during the pseudocapacitance redox reactions [123–125].

Generally, the crystal structure revolution of the electrode materials during the electrochemical process is detected by XRD. However, the phase and surface state of the pseudocapacitive material would rearrange during the charging and discharging process, which leads to the variation of electrochemical active sites on the raw material [126]. Thus, it is hard to reveal the electrochemical reaction process from an atom perspective through the normal XRD test. The resolution of synchrotron XRD is an order of magnitude higher than that of laboratory XRD, which makes it easier to avoid the overlapping of the diffraction peaks and raise the quality of the diffraction data. Thus, synchrotron XRD is widely used to explore the undetectable phase transformation during the pseudocapacitive electrochemical process and reconfiguration processes of the raw materials [127–131]. Additionally, XPS analysis is always employed to help investigate the reaction mechanism of the pseudocapacitive materials through confirming the valence state of elements at different potential during the charging/discharging process [126].

For surface redox pseudocapacitance, the anions and cations in the electrolyte participate in the rapid redox reaction on the surface of the transition metal oxide during the electrochemical process [132,133]. The potential of the electrode obeys a linear relation with the charge and a proportional relation with the feasible area of the electrode surface exposing to active ions [126,133]. When the reaction mechanism under the redox peaks is unclear, hard XAS can identify the redox species directly. Furthermore, XAS is a widely used technique to explore the mechanism of the intercalation process through detecting the evolution of structural features and electronic properties of MXenes at atomic scale [133–135]. XAS also plays an important role in identification and quantitatively analysis of the faradic reaction in the extrinsic pseudocapacitive process as it is difficult to detect the surface charging process via the conventional characterization tools [136,137].

XAFS can be divided into XANES in the energy range of 30–50 eV near the absorption edge structure and EXAFS in the range of 30–1000 eV or even higher than the absorption edge [133,138]. The shape and position of the absorption edge can provide information on the valence and geometry of the metal elements [133,139]. Thus, XANES can be applied to detect the symmetry, oxidation state, and the steric structure around the absorbing atom [133,140]. EXAFS can further detect the local structural information around the central atom, including atomic spacing, coordination number, and disorder [133,141].

Pair Distribution Function (PDF) analysis based on the data from synchrotron X-ray sources could provide both long-range (>10 nm) atomic structure information and short-range structure information in the material, such as short-range distribution, bond lengths, and local defects [133,142–144]. Thus, PDF analysis of pseudocapacitive electrodes in different states could provide in-depth studies of the variation of the fine structure of the materials and demonstrate the effect of short-range structure to the electrochemical performance of the pseudocapacitive materials [142].

3.3. Simulations

Molecular simulations such as classical molecular dynamics (MD), classical density functional theory (classical DFT), and Monte-Carlo (MC) methods are popular methods to study the energy storage of electric double-layer structure in different electrode geometries

and electrolyte components [145]. DFT is commonly applied to calculate the energy barrier for the ion migrating onto the surface or diffusing into the inner space of the electrode materials [146,147]. The lower energy barrier demonstrates the smoother diffusion path of the ions and fast redox reaction kinetics [148]. The feature of interface is always complex and changeable, which makes it quite difficult to simulate the pseudocapacitive behavior. The simulation of pseudocapacitive behavior is mainly conducted in two ways: (a) describing the solid/liquid interface under specific limiting conditions via numerical solution and scaling analysis with classical equations (for instance, PNP and PB equations) [145]; (b) atomistic modeling based on quantum mechanics and molecular mechanics [145].

Zhang's team reported an amorphous TiO_2 featured with titanium vacancies and open channels in the nanostructure [149]. In order to elucidate the pseudocapacitive storage mechanism thoroughly, structural simulations of the amorphous TiO_2 and anatase- TiO_2 during the Li^+ storage process were conducted based on DFT. Firstly, they confirmed the existence of abundant bridging hydroxyl groups in the bulk and surface of the amorphous TiO_2 (Figure 4a,b) and the spacing between the neighboring titanium atoms as being larger than that of the anatase- TiO_2 (Figure 4c,d). Then, thermodynamic stability was analyzed by simulating the structure of the samples before and after the Li^+ insertion (Figure 4e,f). The lithiation energy corresponding to the Li^+ insertion process involved the titanium vacancies and open framework being lower than that of the anatase- TiO_2 , which indicated that the vacancies and open framework facilitate the pseudocapacitive storage [149]. The movement route of the Li^+ in the bulk model for the two samples were investigated, which demonstrated that the energy barrier of the Li^+ transfer from the surface to the inner reaction site and the reaction heat corresponding to Li^+ migration in amorphous TiO_2 with vacancies is lower. Furthermore, the energy calculation convincingly revealed the fast kinetic and thermodynamically favorable reaction nature brought by the pseudocapacitive storage. All these results comprehensively explained the pseudocapacitive storage process was closely associated with the vacancies and open framework in the amorphous TiO_2 [149].

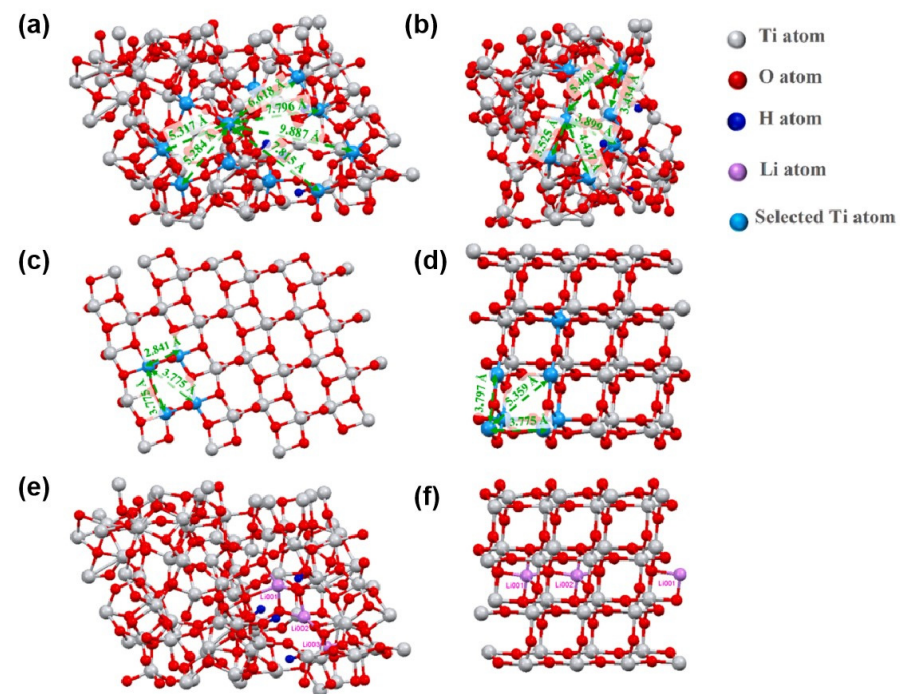


Figure 4. Structural models of amorphous titanium oxide (a,b) and anatase TiO_2 (c,d) [149]. Structural models of amorphous titanium oxide (e) and anatase TiO_2 (f) after Li^+ insertion. The light blue spheres stand for the selected Ti atoms in open channels [149]. Copyright 2023, Elsevier.

3.4. First-Principles Calculations

Zhang et al. designed a hierarchical $\text{VS}_2/\text{Ti}_3\text{C}_2\text{T}_x$ MXene hybrid and demonstrated the significant intercalation pseudocapacitance mechanism, which led to high specific capacity, fast charging capability, and long lifespan [150]. They conducted electrochemical kinetic analysis to demonstrate the smooth insertion of Na^+ and the existence of intercalation pseudocapacitance mechanism. Furthermore, the adsorption energy of Na^+ on the surface and in the layer of VS_2 were calculated to be -3.24 and -3.29 eV based on the first-principle, respectively (Figure 5a,b). These results further indicated the Na^+ is easy to insert into the interlayer and on the surface of the VS_2 , which supports the intercalation pseudocapacitive storage and facilitates the high rate performance of the $\text{VS}_2/\text{Ti}_3\text{C}_2\text{T}_x$ MXene [150].

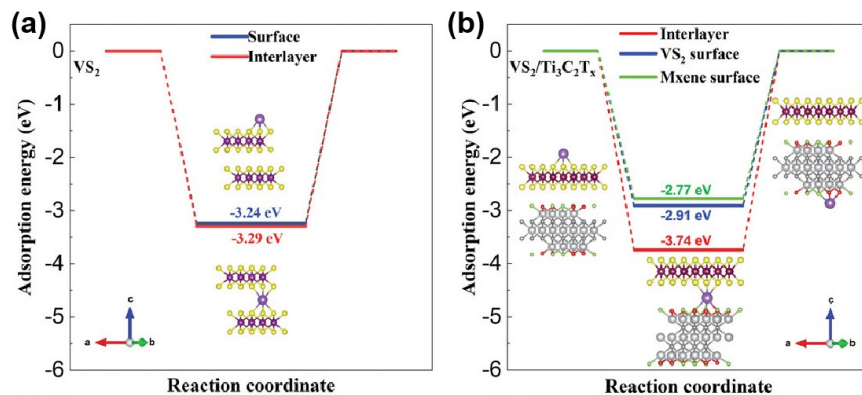


Figure 5. Theoretical calculations. Adsorption energy of one Na atom adsorbed on the surfaces and in the layers of (a) VS_2 - VS_2 and (b) $\text{VS}_2/\text{Ti}_3\text{C}_2\text{T}_x$ [150]. Copyright 2023, Wiley.

These methods are generally applied comprehensively to accurately trace the phase evolution and crystal change accompanying the pseudocapacitive storage process. Zeng et al. developed a surface redox pseudocapacitance-based vanadium nitride (VN) nanoparticle, which delivers a superior discharge capacity of 204 mAh/g at 0.1 A/g after 500 cycles and 132.6 mAh/g at 1.0 A/g after 6600 cycles [133]. They confirmed that the redox reactions only occur on the surface of the VN electrode without phase transformation through ex situ XRD (Figure 6a), ex situ Raman (Figure 6b), and ex situ XPS (Figure 6c). Density functional theory (DFT) calculations were also applied to thoroughly explain the surface pseudocapacitive mechanism (Figure 7). During the sodiation/desodiation process, the XRD patterns of the VN@CF almost remain the same, which illustrated that conversion reaction hardly happened. The Raman spectra of the VN@CF at various states showed almost the same peak position, shape, and I_D/I_G , revealing that no phase and structural transformation happened during the charging/discharging process. The ex situ XPS spectra of V2p and N1s confirmed that the N sustained the valence of -3 during the charging/discharging process while the V^{3+} was slightly reduced to $\text{V}^{(3-x)+}$ at a discharge voltage of 1 V. The sodiation process can be described as $\text{VN} + x\text{Na} = \text{Na}_x\text{VN}$, with high reversibility and accompanied by significant surface redox pseudocapacitive capacity (Figure 6d). The DFT calculation indicated that the energy barrier for Na^+ migrating onto the surface of VN@CF (~ 0.6 eV) is much lower than that for Na^+ diffusing into the inner space (15.33 eV). Such a low energy barrier accounted for the dominated surface redox pseudocapacitance and greatly contributed to the stable cyclicity and high rate performance [133].

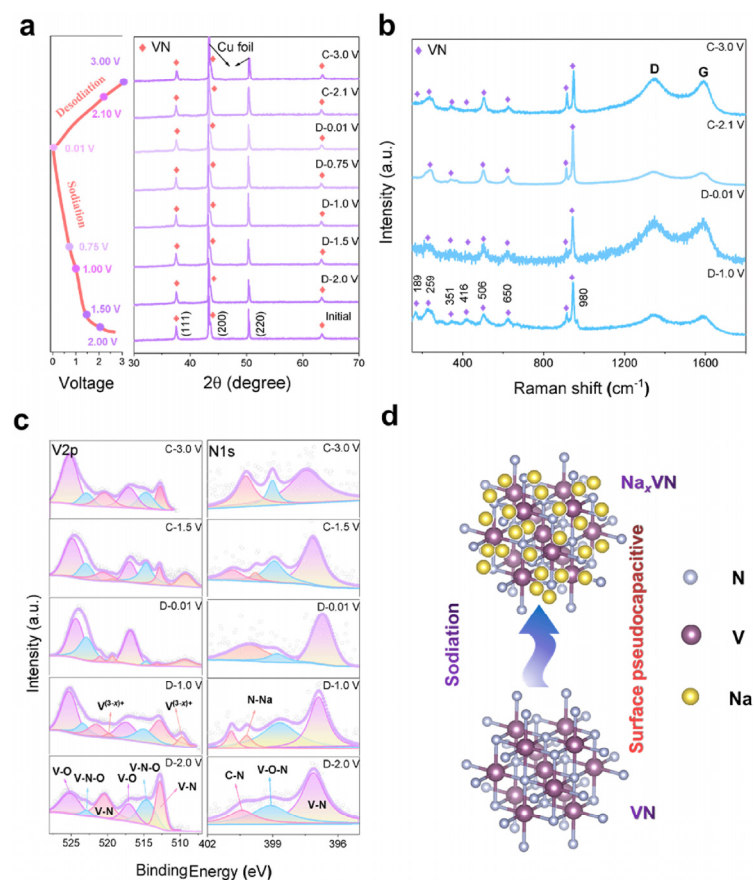


Figure 6. (a) Charge/discharge profiles of VN@CF at 0.1 A/g and corresponding ex situ XRD patterns. (b) Ex situ Raman spectra. (c) Ex situ XPS spectra of V2p and N1s. (d) The schematic illustration for the Na⁺ storage behavior [133]. Copyright 2023, Elsevier.

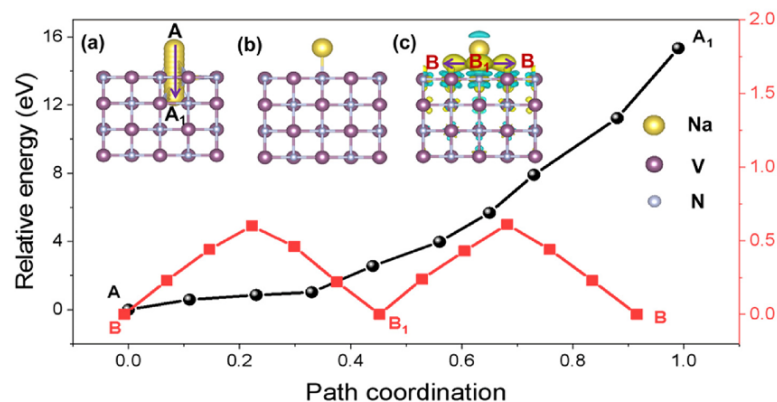


Figure 7. DFT calculations of relative energy variations along two migration paths. The insets display the Na-ions insertion path into the (a) VN bulk ($A \rightarrow A_1$), (b) optimal Na ions adsorption onto (002) plane of VN, and (c) Na-ions diffusion between two neighboring sites (B/B1), respectively [133]. Copyright 2023, Elsevier.

4. Designing Strategies and Methods to Enhance Pseudocapacitance

The pseudocapacitive contribution is adjustable by designing the size, morphology, composition, or structure of the electrode. Features beneficial for high pseudocapacitance are as follows: (i) Nanostructure provides a shortened diffusion pathway, and the small-size effect helps enhance the electrochemical reaction kinetics during lithiation–delithiation process. (ii) An optimized surface and nanocrystal interface guarantees sufficient contact area between the electrode and electrolyte, which are favorable for kinetic enhancement

of interfacial ion diffusion. (iii) Plentiful structural defects, such as of vacancies, point defects, dislocations, stratification and grain boundaries, can significantly promote Li-ion diffusion kinetics, which is vital for high pseudocapacitance. (iv) Element doping can bring about surface defects and supply extraordinary sites for surface pseudocapacitive storage. (v) Proper component modification may raise the pseudocapacitive contribution to total capacity. These advantages help bring about optimal conditions for the pseudocapacitive electrochemical process [85,151].

4.1. Nanostructure Designing

The pseudocapacitive effect can be brought in traditional electrode materials through designing a beneficial nanostructure convenient for high levels of redox and surface pseudocapacitance [49]. Generally, nanostructure would introduce a nanometer size effect, which causes drastic changes in the physical and chemical properties of the material when their size are reduced to nanoscale [109–111,152]. Consequently, the electrochemical behavior of electrodes changes gradually from diffusion-dominant behavior to surface-confined pseudocapacitive nature as the structure changes from bulk to nanoscale [20,152,153]. The origin of the transition lies in the diffusion length reduction and surface area enlargement caused by the size minimization, which would efficiently facilitate the non-insertion charge storage process [154,155].

Masashi's team demonstrated that the crystalline size of the electrode had a significant effect on its electrochemical performance. His team found that the LiCoO₂ electrode yielded a distinct transition from diffusion-controlled to pseudocapacitive behavior with a reduction in particle sizes [80]. The discharge curve of LiCoO₂ displays an evident plateau, indicating the typical battery-type behavior in bulk material. Subsequently, the plateau vanished as the size reduced, which is attributed to the transformation to the pseudocapacitance dominating behavior of the electrode. However, this phenomenon was not thoroughly comprehended and well explained at the time, thus, the relevance between extrinsic pseudocapacitance and the nanosize transition effect was not established. The cathode materials with nanosize structure generated capacitive behavior during electrochemical testing, which displayed the almost linear galvanostatic charging/discharging curves as the particle size decreased [35].

Chen's team synthesized FeS₂ microspheres constituting tightly aggregated nanoparticles with a diameter of about 200 nm. The FeS₂ microspheres showed significant pseudocapacitance behavior in SIBs once the electrolyte and voltage window were properly adjusted to permit the intercalation reaction while forbidding the conversion reaction [156]. Later, several structurally modified materials, including V₂O₅ [79] and CeO₂ [157], were found to generate extrinsic pseudocapacitive behavior. In 2022, Raha et al. reported that the electrochemical energy storage mechanism of V₂O₅ transformed into pseudocapacitance-dominated pattern through modifying the structure by optimizing the reaction pressure. As the particle size decreased, the evident redox peaks observed in the CV curves gradually became explanatory, revealing the anticipative translation to pseudocapacitive nature for the electrode [79].

Kim and his teammates reported cation-exchanged vanadium-substituted Keggin-type molybdenum-based polyoxometalates (XPMoV) with an anisotropic rodlike structure, which yielded a pillar effect on the chemical and structural integrity as cathode for Zinc-ion cathode. The surface-confined electrochemical process dominated the charge process and the resulting intercalation pseudocapacitance mechanism took place after the activation process by co-intercalation of Li⁺ and Zn²⁺ ions. The b values of KPMoV at each redox peak were close to 1, demonstrating that the pseudocapacitance dominated the charge storage. Furthermore, the ex situ XRD and XPS spectra confirmed that the three main

planes of the KPMoV are not involved in phase transformation during the reversible Zn^{2+} (de)-intercalation pseudocapacitance upon charging and discharging [158,159]. Thus, nanostructures may bring in pseudocapacitive storage and increase the capacitive contribution of the electrode [48].

4.2. Surface and Interface Modification

Designing a beneficial surface and interface of the electrode could supply sufficient contact area between the electrode and electrolyte, serving as a fluent channel for ion diffusion and electrochemical reaction. According to Brunce Dunn's report, pseudocapacitance can be enhanced by applying a thin-film structure with interconnected mesoporosity and highly oriented crystalline walls with van der Waals gaps. The mesoporous structure enhances the redox pseudocapacitance by facilitating the permeation of the electrolyte to supply more active electrochemical sites and shorter ion diffusion length. The intercalation pseudocapacitance is associated with the iso-oriented crystalline domains and the flexible nanoporous architecture [103].

Furthermore, developing 2D nanostructure is an efficient way of increasing pseudocapacitive contribution. Zhang et al. designed a hierarchical 2D $VS_2/Ti_3C_2T_x$ MXene hybrid, where the VS_2 nanopetals are finely anchored on the surface or among the layers of the 2D conductive $Ti_3C_2T_x$ microplates via stable chemical bonds (Figure 8a) [150]. Such a structure could efficiently facilitate Na^+ insertion, promote ion transportation, forbid the excessive local Na^+ insertion, and guarantee the reversible insertion/deinsertion. Synthetically, the $VS_2/Ti_3C_2T_x$ hybrid obtained significant intercalation pseudocapacitive behavior based on the high reversibility and fast kinetic of the Na^+ insertion. The intercalation pseudocapacitance storage is confirmed to be dominated by the adsorption and contribute a large proportion of the total storage. Thus, the $VS_2/Ti_3C_2T_x$ hybrid displayed high rate capacity and superior long-term all-climate cycling performance [150]. Liu's team reported a special 2D polypyrrole-coated NiS_2 nanplatelets ($NiS_2@PPy$) with porous NiS_2 nanplatelets coated by polypyrrole and studied the performance as an electrode for SIBs. In this structure, the ion and electron transportation were highly accelerated, which resulted in the decrease of the charge transfer impedance of the electrochemical reaction. These merits significantly encouraged the reversible faradic storage process occurring on the surface and interface of the electrode, which denoted interfacial pseudocapacitive effect storage. Even at a low scan rate of 0.1 mV/s, the interfacial pseudocapacitive storage contributed nearly 90% of the total storage. The $NiS_2@PPy$ electrode achieved high specific capacity of 393 and 373 mAh/g at a current density of 2 and 5 A/g (Figure 8b) [160].

However, high surface area is not the unique determinant for pseudocapacitance; interface modification could also efficiently encourage the pseudocapacitive behavior. Chen and his teammates reported an anatase TiO_2 nanosheets with significant pseudocapacitance behavior, but the specific surface area was only $32\text{ m}^2/\text{g}$. This phenomenon was associated with the abundant nanograins boundary in the anatase TiO_2 nanosheets, which supply plentiful active sites for accumulation of ion/electron. Thus, the pseudocapacitive storage could happen at the nanocrystal interface as well as on the surface of the electrode [161]. Zhao et al. introduced fast surface-redox pseudocapacitance charge storage in magnesium batteries through interface reconstruction by modifying the TiO_2 cathode with ultrathin carbon coating and oxygen vacancies. The improved cathode/electrolyte interface efficiently circumvented the sluggish migration of Mg^{2+} into the solid-phase and facilitate remarkable rate performance and long lifespan [162].

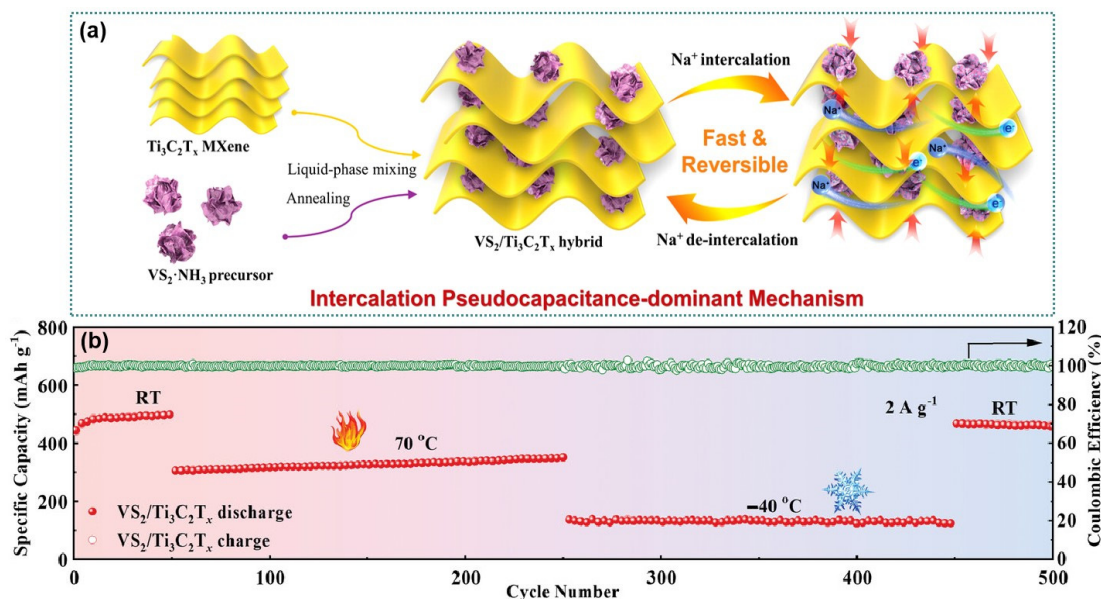


Figure 8. (a) Preparation process and storage mechanism of the $\text{VS}_2/\text{Ti}_3\text{C}_2\text{T}_x$ hybrid [150]. Copyright 2023, Wiley. (b) All-climate long-term cycle performance of $\text{VS}_2/\text{Ti}_3\text{C}_2\text{T}_x$ at 70 and -40 $^{\circ}\text{C}$ at 2 A g^{-1} [150]. Copyright 2023, Wiley.

4.3. Defects

Defects enlarge the pseudocapacitive contribution through supplying a wider diffusion route and accelerating the reaction kinetics. In 2016, Bruce Dunn's team found that introducing oxygen vacancies to the $\alpha\text{-MoO}_3$ enabled the LIBs to obtain higher pseudocapacitive storage capacity. The oxygen vacancies could increase the van der Waals gap, resulting in optimized electrochemical kinetic. The increased van der Waals gap was demonstrated by the raised b -lattice cell parameter and DFT calculation [163]. An amorphous TiO_2 with titanium vacancies and open channels was synthesized by Zhang et al. [164]. They confirmed the existence of pseudocapacitive behavior in a series of samples based on the b values of each sample by analyzing the CV curves. The b value of the amorphous TiO_2 turned out to be higher than anatase TiO_2 at the voltage ranging from 0 to 3 V, indicating more significant capacitive behavior during the charging/discharging process. The pseudocapacitive contribution ratio to the total capacity of the amorphous TiO_2 was also higher than that of anatase TiO_2 . In order to ascertain the reason for the higher pseudocapacitive contribution of the amorphous TiO_2 , they performed theoretical simulation using DFT to elucidate the reaction kinetics during the Li^+ storage. The structure analysis demonstrated that the amorphous contains plenty of bridging hydroxyl groups in the bulk and surface, which would induce and stabilize titanium vacancies in TiO_2 . The equilibrium structures of all the atoms in the amorphous TiO_2 were relaxed. Furthermore, the spacing between neighboring titanium atoms in the amorphous TiO_2 was broader than that of the anatase TiO_2 . These results indicated that the amorphous TiO_2 could provide an open Li^+ diffusion pathway and fast transportation, which guarantee a rapid reaction kinetic [164].

Cai Yi's team reported an amorphous manganese dioxide with abundant oxygen vacancies and void spaces, which exhibited enhanced pseudocapacitive storage in ZIBs [165]. Zhang et al. demonstrated the significant pseudocapacitive storage by tracing the migration pathway of $\text{H}^+/\text{Zn}^{2+}$ in the M phase VO_2 based on the band valence method. The pseudocapacitive storage was dependent on the H^+ insertion into the electrode. Venkata Sai Avvaru and his team reported that Co_3O_4 nanosheets with plentiful defects including

vacancies, dislocations and grain boundaries, showed a 2.6 times higher pseudocapacitive contribution than the defect-free Co_3O_4 nanosheets in LIBs [166,167].

4.4. Heteroatom Doping

Heteroatom doping was confirmed to be effective in enhancing the pseudocapacitive behavior. Chen's team proposed a simple and novel strategy to adjust the surface structure of few-layered MXene flakes via doping a small amount of Nb element. The strong bond between Nb and O elements enabled the $\text{V}_{1.8}\text{Nb}_{0.2}\text{CT}_x$ and $\text{Ti}_{2.7}\text{Nb}_{0.3}\text{C}_2\text{Tx}$ solid-solution MXene gain enhanced pseudocapacitance performance because of much fewer $-\text{F}$ functional groups and a higher O content [168]. Zhu et al. reported a P-doped carbon nanotube/reduced graphene oxide aerogel cathode for high power and energy zinc ion storage. The doped P was proved to have a positive role in enlarging the interlayer spacing of P-CNT/rGO and enhancing the pseudocapacitance reactions [169]. Ding and his team developed a $\text{Fe}_2\text{O}_3/\text{MoC@NG}$, which featured a hierarchical mesoporous 3D structure and abundant strong interfacial covalent bonds of Fe-O-Mo, Mo-C and Fe/Mo-N. The electrode achieved a lifted diffusion coefficient of Li^+ and enhanced pseudocapacitance behavior, which resulted in rapid electrochemical reaction kinetics. The contribution of pseudocapacitance to the total storage in the assembled full LIBs was calculated based on the CV curves of various scan rates. The Li^+ diffusion along with the hetero-interface proved to be dominated by the pseudocapacitance mechanism [170]. Ji's team reported a hydrated vanadium oxide displaying pseudocapacitive behavior with the assistance of interlayer doped Mn^{2+} . The interlayer space of the V-based oxides was broadened due to the solid pillars formed via the combination of Mn^{2+} with oxygen in VO_6 octahedron of V-based oxides layers. The Mn^{2+} doping was confirmed to support the pseudocapacitive behavior and increase the capacitive contribution to the total capacity [171].

4.5. Component Modification

Proper component modification may cause the rise in pseudocapacitive contribution to total capacity. For example, Mitchell et al. reported that the pseudocapacitive behavior of $\text{WO}_3 \cdot 2\text{H}_2\text{O}$ vanished with the removal of the H_2O component, which demonstrates that the extrinsic pseudocapacitive behavior was affected by the electrode component [172]. As $\text{WO}_3 \cdot \text{H}_2\text{O}$ transforms to anhydrous WO_3 , the b value decreases from 0.9 to 0.6 and 0.4, confirming the weakening in pseudocapacitive contribution. The less reversible current peaks become predominant in the CV curves of anhydrous WO_3 compared with the redox peaks in $\text{WO}_3 \cdot \text{H}_2\text{O}$, revealing the advantage for $\text{WO}_3 \cdot \text{H}_2\text{O}$ in capacity retention.

5. Advanced Applications

Flexible EES devices are drawing the increasing attention of researchers due to expanding demand for portable and wearable electronic devices. The flexible EES devices call for flexible electrode or pseudocapacitive materials with superior mechanical strength, stable electrochemical properties, and superior conductivity, which are essential for high capacity and stable cycling performance [173–176]. However, traditional electrodes, consisting of active materials, binders, and conductive carbon additives, always obtain poor mechanical robustness. Layered materials, possessing a soft and elastic nature due to the long-lasting Van der Waals forces within the stacked layers, are believed to be a suitable flexible electrode [177–179]. Layered carbon-based materials, such as graphene, carbon nanotube paper, and carbon cloth, display excellent conductivity and durable mechanical strength to withstand repeated bending, folding and rolling. However, single carbon materials only obtain limited capacitance due to the low package density and high porosity. The introduction of pseudocapacitive materials, e.g., transition metal oxides/hydroxides

or conductive polymers is an ideal solution to promote the electrochemical performance of the carbonaceous electrode materials. Hybrid nanocomposite constructed by loading pseudocapacitive materials, such as, MnO_x , RuO_2 , polyaniline, and polypyrrol, on the flexible carbon substrate enable high conductivity, excellent electrochemical performance, and structural flexibility [180–183].

5.1. Flexible Supercapacitor

Jia's team proposed a novel all-in-one flexible supercapacitor (AFSC) with an “all-graphene” structure [184]. With the benefit of the additional pseudocapacitance enhancement of methylene blue (MB) molecules, the AFSC, assembled with the flexible self-supporting MB modified graphene hydrogel film (MB/rGO) obtained by a simple hydrothermal as electrode and graphene oxide (GO) as separator, exhibited a high specific capacitance of 317.27 F/g at 0.2 A/g. Even at a high current density of 20 A/g, the specific capacity still maintained 213.66 F/g. Furthermore, the soft package AFSC device exhibited excellent mechanical flexibility [184].

Kaur's team reported a flexible symmetric supercapacitor (FSSC) device composed of titanium chromium nitride (Ti-Cr-N) nanocomposite possessing uniform distributed nanoparamids deposited directly over flexible stainless-steel mesh (SSM) via reactive magnetron co-sputtering [185]. The Ti-Cr-N/SSM thin-film electrodes (TFEs) were optimized through adjusting the titanium concentration in the Ti-Cr-N thin films. Due to the enhanced synergism of improved electrical conductivity, higher ionic conductivity, and increased surface area, the Ti-Cr-N/SSM TFEs delivered an excellent specific capacitance of 263.75 F/g (or 40.3 mF/cm²) at 0.32 A/g. What is noteworthy is that they confirmed the dominating existence of surface-limited capacitive and pseudocapacitive storage mechanisms. Furthermore, the assembled Ti-Cr-N/SSM || Ti-Cr-N/SSM FSSC device manifested a high energy density of 9.27 Wh/kg and power density of 13.71 kW/kg while maintaining 82.32% electrochemical stability after 4500 cycles. The Ti-Cr-N nanoparamid demonstrated superior resilient structural strength with a remarkable mechanical stability of 90% at a 90° bending angle for the FSSC over 600 GCD cycles [185].

5.2. Quasi-Solid-State Battery

A quasi-solid-state battery is a battery in which a small amount of liquid electrolyte (usually less than 5 wt.%) is added to an all-solid-state battery. Most of the electrolyte is a solid electrolyte, and the mass and volume of the solid electrolyte are greater than that of the electrolyte. Quasi-solid-state batteries add a small amount of liquid electrolyte on the basis of all-solid-state batteries, and these liquid electrolytes are mainly used to infiltrate the interface. Compared with liquid batteries, quasi-solid-state batteries still retain the diaphragm, but the diaphragm is coated with a solid electrolyte coating, thus improving the safety of the battery.

Liu's team reported a quasi-solid-state flexible self-healing secondary battery using hydrogel-based water-in-salt electrolyte and electrochemically deposited electrodes [186]. The designed VO_2 nanobelts were coated with polyaniline (PANI) grown on a carbon cloth (CC) as anode material ($\text{VO}_2@\text{PANI}/\text{CC}$). The $\text{VO}_2@\text{PANI}/\text{CC}$ electrode gained an 85.4% capacitive contribution at scan rate 1.0 mV/s. It cooperated with the water-in-salt electrolyte with photoinitiated polymerization of acrylamide in ZnCl_2 solution. The batteries gained both excellent electrochemical properties and high recovery performance after bending/cutting, which enable the quasi-solid-state battery to have good capability for flexible and portable electronics. The faradaic process determined by surface redox reactions is conducive to the enhancement of rate performance and long-term stability under high current densities.

Ren's team developed a two-dimensional cation-deficient Cu-Bi_{2-x}Se₃ with an ultrathin size of about 4 nm and appropriate Bi-vacancies generated by Cu doping (Figure 9) [187]. Attributed to Bi-vacancies, the Cu-Bi_{2-x}Se₃ possessed improved conductivity, boosted Zn²⁺ adsorption energy, a lower Zn²⁺ migration barrier, and larger lattice plane offsets. Additionally, the ultrathin 2D nanostructure decreased the Coulombic ion-lattice repulsion and raised the bulk and surface conductivity. They demonstrated that the Cu-Bi_{2-x}Se₃ achieved high specific capacity and enhanced rate performance as a cathode for Zn-ion batteries. The application as cathode material for quasi-solid fiber-shaped Zn-ion batteries was explored by using the polyacrylamide/zinc sulfate (PAM/ZnSO₄) hydrogel as electrolyte and Zn fiber as anode. The quasi-solid fiber-shaped CuBi_{2-x}Se₃//Zn battery displayed favorable cycling performance, exceptional flexibility, and durable machinability. The two-fiber-shaped battery can be connected in series and woven into cloth to power an electronic watch for a period of time, which demonstrates a promising application in wearable electronic devices [187].

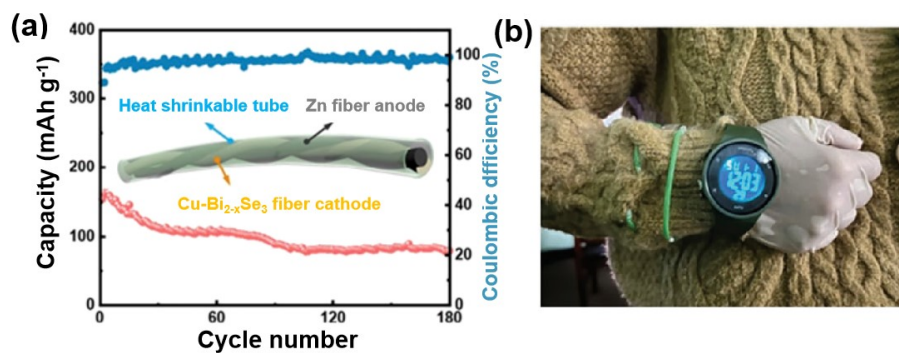


Figure 9. (a) The cycle performance of quasi-solid fiber-shaped Cu-Bi_{2-x}Se₃//Zn battery at 0.05 A/g; the inset is the schematic illustration of the as-prepared fiber-shaped battery [187]. (b) Photograph of the flexible fiber-shaped Cu-Bi_{2-x}Se₃//Zn battery wearable application [187]. Copyright 2023, Wiley-VCH.

6. Summary and Outlook

Pseudocapacitive electrode materials demonstrate the potential to realize high energy and high power in EES for storage, combining the merits of diffusion-controlled and capacitance-controlled processes. In this review, the foundational theories involving pseudocapacitive materials, including diffusion principles and storage mechanisms, and their classification, were elaborated. The latest methods and techniques of identifying pseudocapacitive material and quantitatively analyzing their contribution to total storage were discussed. Furthermore, we discussed modification strategies to enhance the pseudocapacitive storage of electrodes and introduced some advanced application devices, except for batteries. Developing materials with typical structural characteristics, such as high specific area, plentiful vacancies, hybridization and element doping, is a significant method for introducing or enhancing pseudocapacitive storage. Employing pseudocapacitive electrode materials in EES would achieve sufficiently stable reversibility, high power, and ideal fast-charging performance. Based on the above-mentioned theoretical foundations and analysis methods, pseudocapacitive materials should be more widely applied and further developed in the future. The following proposed viewpoints may be significant in enlarging the contribution of pseudocapacitive materials to high-performance EES.

- (1) Surface modification and interface engineering are efficient methods of introducing or enhancing pseudocapacitive storage. The solvation/desolvation of ions under fast-charging operating conditions could become the speed control step of the whole process, which closely relies on the interfacial chemistry of the electrode material.

Optimizing the electrode/electrolyte interface with excellent ion conductivity and mechanical stability would enable rapid reaction kinetics in the pseudocapacitive storage. Thus, it is of great significance to try more innovative and practical ways to design electrodes with a beneficial surface and electrode/electrolyte interface, which would enable a fluent and stable electrochemical transformation process.

- (2) Although the theories about the pseudocapacitance are enough for researchers to recognize pseudocapacitive behavior, further deep insight and more overall understanding are essential. Describing the relationship of electrode/electrolyte interfacial properties and the ion solvation behavior based on the laws of thermodynamics may be meaningful in revealing the essence of the pseudocapacitive process. Furthermore, conducting molecular simulation at the interface may also help to understand pseudocapacitive behavior.
- (3) Accuracy improvement in time resolution for in situ characterization: the pseudocapacitive materials store energy in quite a short time (several seconds) through the special energy conversion process. However, in some circumstances, the charging rate must be set slower during the in situ synchrotron measurements to obtain more useful data. The unmatched charging rate would lead to an inaccurate manifestation of some ultra-high-rate pseudocapacitive storage processes. Employing the ultra-powerful third-generation synchrotron light source in the in situ measurement could help to acquire sufficient measurement signals in a very short time. In this way, the pseudocapacitive storing process can be tracked in real-time through the high time-resolved synchrotron spectra.
- (4) The pseudocapacitive behavior with large mass loading has to be considered before practical utilization. Pseudocapacitance was proven to be a hybrid energy storage mechanism that combines the merits of different EES devices, which greatly enhance the rate performance of EES devices. Obtaining maximum performance under per unit mass load is a precondition that must be solved before realizing large-scale commercial application. Large electrode surface areas are essential to guarantee sufficient reaction sites and smooth ion transmission crossing the electrode–electrolyte interface. Thus, the densification and the large specific area of the electrode must be properly balanced during the design of the electrode.

Author Contributions: Conceptualization, methodology, investigation, validation, writing—review and editing, supervision X.R. Conceptualization, methodology, investigation, validation, writing and editing, Z.L. All authors have read and agreed to the published version of the manuscript.

Funding: This work was supported by Nanyang Normal University (2022ZX007, 2023PY014).

Data Availability Statement: Data are available upon request.

Acknowledgments: This work was financially supported by Nanyang Normal University.

Conflicts of Interest: The authors declare no conflict of interest.

References

1. Zhan, R.; Wang, X.; Chen, Z.; Seh, Z.W.; Wang, L.; Sun, Y. Promises and challenges of the practical implementation of prelithiation in lithium-ion batteries. *Adv. Energy Mater.* **2021**, *11*, 2101565. [[CrossRef](#)]
2. Xie, L.; Tang, C.; Bi, Z.; Song, M.; Fan, Y.; Yan, C.; Li, X.; Su, F.; Zhang, Q.; Chen, C. Hard carbon anodes for next-generation Li-ion batteries: Review and perspective. *Adv. Energy Mater.* **2021**, *11*, 2101650. [[CrossRef](#)]
3. Zhang, L.; Li, X.; Yang, M.; Chen, W. High-safety separators for lithium-ion batteries and sodium-ion batteries: Advances and perspective. *Energy Storage Mater.* **2021**, *41*, 522–545. [[CrossRef](#)]
4. Chen, Y.; Kang, Y.; Zhao, Y.; Wang, L.; Liu, J.; Li, Y.; Liang, Z.; He, X.; Li, X.; Tavajohi, N. A review of lithium-ion battery safety concerns: The issues, strategies, and testing standards. *J. Energy Chem.* **2021**, *59*, 83–99. [[CrossRef](#)]
5. Zhou, W.; Lu, Q.; Zheng, Y. Review on the selection of health indicator for lithium ion batteries. *Machines* **2022**, *10*, 512. [[CrossRef](#)]

6. Neau, F.; Chiric, I.M.; Borbáth, I.; Tálas, E.; Tompos, A.; Somacescu, S.; Osiceanu, P.; Folgado, M.A.; Chaparro, A.M. Recent progress on electrocatalysts and electrodes for portable fuel cells. *J. Mater. Chem. A* **2021**, *9*, 17065–17128. [[CrossRef](#)]
7. Xiao, F.; Wang, Y.C.; Wu, Z.P.; Chen, G.; Yang, F.; Zhu, S.; Siddharth, K.; Kong, Z.; Lu, A.; Li, J.C.; et al. Recent advances in electrocatalysts for proton exchange membrane fuel cells and alkaline membrane fuel cells. *Adv. Mater.* **2021**, *33*, 2006292. [[CrossRef](#)]
8. Wayu, M. Manganese oxide carbon-based nanocomposite in energy storage applications. *Solids* **2021**, *2*, 232–248. [[CrossRef](#)]
9. Bokhari, S.; Siddique, A.H.; Sherrell, P.C.; Yue, X.; Gao, W. Advances in graphene-based supercapacitor electrodes. *Energy Rep.* **2020**, *6*, 2768–2784. [[CrossRef](#)]
10. Burke, A.F.; Zhao, J. Past, Present and future of electrochemical capacitors: Technologies, performance and application. *J. Energy Storage* **2021**, *35*, 102310. [[CrossRef](#)]
11. Ho, J.; Jow, T.R.; Boggs, S. Historical introduction to capacitor technology. *IEEE Electr. Insul. Mag.* **2010**, *26*, 20–25. [[CrossRef](#)]
12. Sinha, P.; Kar, K.K. Introduction to supercapacitors. In *Handbook of Nanocomposite Supercapacitor Materials II*; Springer Series in Materials Science; Springer: Berlin/Heidelberg, Germany, 2020; Volume 302, pp. 1–28.
13. Chodankar, N.R.; Pham, H.D.; Nanjundan, A.K.; Fernando, J.F.S.; Jayaramulu, K.; Golberg, D.; Han, Y.-K.; Dub, D.P. True meaning of pseudocapacitors and their performance metrics: Asymmetric versus hybrid supercapacitors. *Small* **2020**, *16*, 2002806. [[CrossRef](#)]
14. Forouzandeh, P.; Kumaravel, V.; Pillai, S.C. Electrode materials for supercapacitors: A review of recent advances. *Catalysts* **2020**, *10*, 969. [[CrossRef](#)]
15. Shen, F.; Sun, Z.; He, Q.; Sun, J.; Kaner, R.B.; Shao, Y. Niobium pentoxide based materials for high rate rechargeable electrochemical energy storage. *Mater. Horiz.* **2021**, *8*, 1130–1152. [[CrossRef](#)] [[PubMed](#)]
16. Herrero, E.; Buller, L.J.; Abruna, H.D. Underpotential deposition at single crystal surfaces of Au, Pt, Ag and other materials. *Chem. Rev.* **2001**, *101*, 1897–1930. [[CrossRef](#)]
17. Li, C.; Balamurugan, J.; Kim, N.H.; Lee, J.H. Hierarchical Zn-Co-S nanowires as advanced electrodes for all solid state asymmetric supercapacitors. *Adv. Energy Mater.* **2018**, *8*, 1702014. [[CrossRef](#)]
18. Conway, B.E.; Gileadi, E. Kinetic Theory of Pseudo-Capacitance and Electrode Reactions at Appreciable Surface Coverage. *Trans. Faraday Soc.* **1962**, *58*, 2493. [[CrossRef](#)]
19. Conway, B.E.; Birss, V.; Wojtowicz, J. The role and utilization of pseudocapacitance for energy storage by supercapacitors. *J. Power Sources* **1997**, *66*, 1–14. [[CrossRef](#)]
20. Xu, Y.; Yun, S.; Yeon, J.S.; Bhattachary, P.; Park, H.S. Emergent pseudocapacitance of 2D nanomaterials. *Adv. Energy Mater.* **2018**, *8*, 1702930.
21. Liu, Y.; Jiang, S.P.; Shao, Z. Intercalation pseudocapacitance in electrochemical energy storage: Recent advances in fundamental understanding and materials development. *Mater. Today Adv.* **2020**, *7*, 100072. [[CrossRef](#)]
22. Lee, H.Y.; Goodenough, J.B. Supercapacitor behavior with KCl electrolyte. *J. Solid State Chem.* **1999**, *144*, 220–223. [[CrossRef](#)]
23. Bélanger, D.; Brousse, T.; Long, J.W. Manganese oxides: Battery materials make the leap to electrochemical capacitors. *ECS Interface* **2008**, *17*, 49–52. [[CrossRef](#)]
24. Xu, C.; Kang, F.; Li, B.; Du, H. Recent progress on manganese dioxide based supercapacitors. *J. Mater. Res.* **2010**, *25*, 1421–1432. [[CrossRef](#)]
25. Augustyn, V.; Simon, P.; Dunn, B. Pseudocapacitive oxide materials for high-rate electrochemical energy storage. *Energy Environ. Sci.* **2014**, *7*, 1597–1614. [[CrossRef](#)]
26. Liu, J.L.; Wang, J.; Xu, C.H.; Jiang, H.; Li, C.Z.; Zhang, L.L.; Lin, J.Y.; Shen, Z.X. Advanced energy storage devices: Basic principles, analytical methods, and rational materials design. *Adv. Sci.* **2018**, *5*, 1700322. [[CrossRef](#)] [[PubMed](#)]
27. Xia, Q.; Yang, H.; Wang, M.; Yang, M.; Guo, Q.; Wan, L.; Xia, H.; Yu, Y. High energy and high power lithium-ion capacitors based on boron and nitrogen dual-doped 3D carbon nanofibers as both cathode and anode. *Adv. Energy Mater.* **2017**, *7*, 1701336. [[CrossRef](#)]
28. Karade, S.S.; Lalwani, S.; Eum, J.-H.; Kim, H. Coin cell fabricated symmetric supercapacitor device of two-steps synthesized V_2O_5 nanorods. *Electroanal. Chem.* **2020**, *864*, 114080. [[CrossRef](#)]
29. Dong, X.L.; Yang, Y.; Wang, B.L.; Cao, Y.J.; Wang, N.; Li, P.L.; Wang, Y.G.; Xia, Y.Y. Low-temperature charge/discharge of rechargeable battery realized by intercalation pseudocapacitive behavior. *Adv. Sci.* **2020**, *7*, 2000196. [[CrossRef](#)] [[PubMed](#)]
30. Zhao, R.Z.; Zhang, L.Y.; Wang, C.X.; Yin, L.W. Tetramethyl ammonium cation intercalated layered birnessite manganese dioxide for high-performance intercalation pseudocapacitor. *J. Power Sources* **2017**, *353*, 77–84. [[CrossRef](#)]
31. Zheng, Y.; Zheng, S.; Xue, H.; Pang, H. Metal-organic frameworks for lithium-sulfur batteries. *J. Mater. Chem. A* **2019**, *7*, 3469–3491. [[CrossRef](#)]
32. Gan, Z.H.; Yin, J.Y.; Xu, X.; Cheng, Y.H.; Yu, T. Nanostructure and advanced energy storage: Elaborate material designs lead to high-rate pseudocapacitive ion storage. *ACS Nano* **2022**, *16*, 5131–5152. [[CrossRef](#)]

33. Tan, H.; Feng, Y.; Rui, X.; Yu, Y.; Huang, S. Metal chalcogenides: Paving the way for high-performance sodium/potassium-ion batteries. *Small Methods* **2020**, *4*, 1900563. [[CrossRef](#)]
34. Ding, J.; Hu, W.; Paek, E.; Mitlin, D. Review of hybrid ion capacitors: From aqueous to lithium to sodium. *Chem. Rev.* **2018**, *118*, 6457–6498. [[CrossRef](#)] [[PubMed](#)]
35. Wang, R.; Wang, L.; Liu, R.; Li, X.; Wu, Y.; Ran, F. “Fast-Charging” anode materials for lithium ion batteries from perspective of ion diffusion in crystal structure. *ACS Nano* **2024**, *18*, 2611–2648. [[CrossRef](#)] [[PubMed](#)]
36. Liu, W.W.; Xu, M.; Zhu, M.H. Design of a niobium tungsten oxide/C micro-structured electrode for fast charging lithium-ion batteries. *Inorg. Chem. Front.* **2021**, *8*, 3998–4005. [[CrossRef](#)]
37. Lyu, H.; Li, J.L.; Wang, T.; Thapaliya, B.P.; Men, S.; Jafta, C.J.; Tao, R.; Sun, X.G.; Dai, S. Carbon coated porous titanium niobium oxides as anode materials of lithium-ion batteries for extreme fast charge applications. *ACS Appl. Energy Mater.* **2020**, *3*, 5657–5665. [[CrossRef](#)]
38. Tian, T.; Lu, L.L.; Yin, Y.C.; Li, F.; Zhang, T.W.; Song, Y.H.; Tan, Y.H.; Yao, H.B. Multiscale designed niobium titanium oxide anode for fast charging lithium ion batteries. *Adv. Funct. Mater.* **2021**, *31*, 2007419. [[CrossRef](#)]
39. Yan, L.; Rui, X.; Chen, G.; Xu, W.; Zou, G.; Luo, H. Recent advances in nanostructured Nb-based oxides for electrochemical energy storage. *Nanoscale* **2016**, *8*, 8443–8465. [[CrossRef](#)]
40. Li, S.; Xu, Q.; Uchaker, E.; Cao, X.; Cao, G.Z. Comparison of amorphous, pseudohexagonal and orthorhombic Nb_2O_5 for highRate lithium ion insertion. *Cryst. Eng. Comm.* **2016**, *18*, 2532–2540. [[CrossRef](#)]
41. Liu, H.D.; Zhu, Z.Y.; Yan, Q.Z.; Yu, S.C.; He, X.; Chen, Y.; Zhang, R.; Ma, L.; Liu, T.C.; Li, M.; et al. A disordered rock salt anode for fast-charging lithium ion batteries. *Nature* **2020**, *585*, 63–67. [[CrossRef](#)] [[PubMed](#)]
42. Xia, R.; Sun, C.L.; Wang, Y.; Cunha, D.M.; Peng, H.Y.; Zhao, K.N.; Huijben, M.; ten Elshof, J.E. Enhanced lithiation dynamics in nanostructured $\text{Nb}_{18}\text{W}_{16}\text{O}_{93}$ anodes. *J. Power Sources* **2021**, *482*, 228898. [[CrossRef](#)]
43. Zhang, W.; Seo, D.-H.; Chen, T.; Wu, L.J.; Topsakal, M.; Zhu, Y.M.; Lu, D.Y.; Ceder, G.; Wang, F. Kinetic pathways of ionic transport in fast-charging lithium titanate. *Science* **2020**, *367*, 1030–1034. [[CrossRef](#)] [[PubMed](#)]
44. Wang, T.; He, J.R.; Zhu, Z.; Cheng, X.-B.; Zhu, J.; Lu, B.G.; Wu, Y.P. Heterostructures regulating lithium polysulfides for advanced Lithium-Sulfur batteries. *Adv. Mater.* **2023**, *35*, 2303520. [[CrossRef](#)] [[PubMed](#)]
45. Xie, G.J.; Tan, X.; Shi, Z.Z.; Peng, Y.; Ma, Y.; Zhong, Y.R.; Wang, F.X.; He, J.R.; Zhu, Z.; Cheng, X.B.; et al. SiO_x based anodes for advanced Li-ion batteries: Recent progress and perspectives. *Adv. Funct. Mater.* **2025**, *35*, 2414714. [[CrossRef](#)]
46. Tarascon, J.-M.; Armand, M. Issues and challenges facing rechargeable lithium batteries. *Nature* **2001**, *414*, 359–367. [[CrossRef](#)] [[PubMed](#)]
47. Kim, H.; Park, Y.-U.; Park, K.-Y.; Lim, H.-D.; Hong, J.; Kang, K. Novel transition-metalfree cathode for high energy and power sodium rechargeable batteries. *Nano Energy* **2014**, *4*, 97–104. [[CrossRef](#)]
48. Dunn, B.; Kamath, H.; Tarascon, J.-M. Electrical energy storage for the grid: A battery of choices. *Science* **2011**, *334*, 928–935. [[CrossRef](#)] [[PubMed](#)]
49. George, J.; Balachandran, M. Extrinsic pseudocapacitance: Tapering the borderline between pseudocapacitive and battery type electrode materials for energy storage applications. *J. Energy Storage* **2023**, *74*, 109292. [[CrossRef](#)]
50. Feng, D.Y.; Sun, Z.; Huang, Z.H.; Cai, X.; Song, Y.; Liu, X.X. Highly loaded manganese oxide with high rate capability for capacitive applications. *J. Power Sources* **2018**, *396*, 238–245. [[CrossRef](#)]
51. Jabeen, N.; Hussain, A.; Xia, Q.; Sun, S.; Zhu, J.; Xia, H. High-performance 2.6 V aqueous asymmetric supercapacitors based on in situ formed $\text{Na}_0.5\text{MnO}_2$ nanosheet assembled nanowall arrays. *Adv. Mater.* **2017**, *29*, 1700804. [[CrossRef](#)] [[PubMed](#)]
52. Winter, M.; Brodd, R.J. What are batteries, fuel cells, and supercapacitors? *Chem. Rev.* **2004**, *104*, 4245–4269. [[CrossRef](#)] [[PubMed](#)]
53. Wang, G.; Zhang, L.; Zhang, J. A review of electrode materials for electrochemical supercapacitors. *Chem. Soc. Rev.* **2012**, *41*, 797–828. [[CrossRef](#)] [[PubMed](#)]
54. Long, J.W.; Bélanger, D.; Brousse, T.; Sugimoto, W.; Sassin, M.B.; Crosnier, O. Asymmetric electrochemical capacitors—stretching the limits of aqueous electrolytes. *MRS Bull.* **2011**, *36*, 513–522. [[CrossRef](#)]
55. Shi, F.; Li, L.; Wang, X.; Gu, C.; Tu, J. Metal oxide/hydroxide-based materials for supercapacitors. *RSC Adv.* **2014**, *4*, 41910–41921. [[CrossRef](#)]
56. Jiang, Y.; Liu, J. Definitions of pseudocapacitive materials: A brief review. *Energy Environ. Mater.* **2019**, *2*, 30–37. [[CrossRef](#)]
57. Cougnon, C.; Lebègue, E.; Pognon, G. Impedance spectroscopy study of a catechol-modified activated carbon electrode as active material in electrochemical capacitor. *J. Power Sources* **2015**, *274*, 551–559. [[CrossRef](#)]
58. Ma, F.; Ding, S.; Ren, H.; Liu, Y. Sakura-based activated carbon preparation and its performance in supercapacitor applications. *RSC Adv.* **2019**, *9*, 2474–2483. [[CrossRef](#)]
59. Fan, Z.; Yan, J.; Wei, T.; Zhi, L.; Ning, G.; Li, T.; Wei, F. Asymmetric supercapacitors based on graphene/ MnO_2 and activated carbon nanofiber electrodes with high power and energy density. *Adv. Funct. Mater.* **2011**, *21*, 2366–2375. [[CrossRef](#)]
60. Chang, Y.M.; Wu, C.Y.; Wu, P.W. Synthesis of large surface area carbon xerogels for electrochemical double layer capacitors. *J. Power Sources* **2013**, *223*, 147–154. [[CrossRef](#)]

61. Lu, X.; Shen, J.; Ma, H.; Yan, B.; Li, Z.; Shi, M.; Ye, M. A cost-effective way to maintain metal-doped carbon xerogels and their applications on electric double-layer capacitors. *J. Power Sources* **2012**, *201*, 340–346. [[CrossRef](#)]
62. Guo, J.; Zhang, Q.; Li, Q.; Sun, J.; Li, C.; He, B.; Zhou, Z.; Xie, L.; Li, M.; Yao, Y. Rational design of hierarchical titanium nitride@vanadium pentoxide core–shell heterostructure fibrous electrodes for high-performance 1.6 V nonpolarity wearable supercapacitors. *ACS Appl. Mater. Interfaces* **2018**, *10*, 29705–29711. [[CrossRef](#)] [[PubMed](#)]
63. Ju, H.F.; Song, W.L.; Fan, L.Z. Rational design of graphene/porous carbon aerogels for high-performance flexible all-solid-state supercapacitors. *J. Mater. Chem. A* **2014**, *2*, 10895–10903. [[CrossRef](#)]
64. Dubal, D.P.; Chodankar, N.R.; Caban-Huertas, Z.; Wolfart, F.; Vidotti, M.; Holze, R.; Lokhande, C.D.; Gomez-Romero, P. Synthetic approach from polypyrrole nanotubes to nitrogen doped pyrolyzed carbon nanotubes for asymmetric supercapacitors. *J. Power Sources* **2016**, *308*, 158–165. [[CrossRef](#)]
65. Fan, X.; Peng, Z.; Yang, Y.; Zhou, H.; Guo, X. Atomic H-induced cutting and unzipping of single-walled carbon nanotube carpets with a teepee structure and their enhanced supercapacitor performance. *J. Mater. Chem. A* **2015**, *3*, 10077–10084. [[CrossRef](#)]
66. Choi, C.; Lee, J.A.; Choi, A.Y.; Kim, Y.T.; Lepro, X.; Lima, M.D.; Baughman, R.H.; Kim, S.J. Flexible supercapacitor made of carbon nanotube yarn with internal pores. *Adv. Mater.* **2014**, *26*, 2059–2065. [[CrossRef](#)]
67. Li, W.; Zhang, F.; Dou, Y.; Wu, Z.; Liu, H.; Qian, X.; Gu, D.; Xia, Y.; Tu, B.; Zhao, D. A self-template strategy for the synthesis of mesoporous carbon nanofibers as advanced supercapacitor electrodes. *Adv. Energy Mater.* **2011**, *1*, 382–386. [[CrossRef](#)]
68. Jost, K.; Stenger, D.; Perez, C.R.; McDonough, J.K.; Lian, K.; Gogotsi, Y.; Dion, G. Knitted and screen printed carbon-fiber supercapacitors for applications in wearable electronics. *Energy Environ. Sci.* **2013**, *6*, 2698–2705. [[CrossRef](#)]
69. Ren, J.; Bai, W.; Guan, G.; Zhang, Y.; Peng, H. Flexible and weaveable capacitor wire based on a carbon nanocomposite fiber. *Adv. Mater.* **2013**, *25*, 5965–5970.
70. Zhang, L.L.; Zhao, X.; Ji, H.; Stoller, M.D.; Lai, L.; Murali, S.; McDonnell, S.; Cleveger, B.; Wallace, R.M.; Ruoff, R.S. Nitrogen doping of graphene and its effect on quantum capacitance, and a new insight on the enhanced capacitance of N-doped carbon. *Energy Environ. Sci.* **2012**, *5*, 9618–9625. [[CrossRef](#)]
71. Wu, Z.S.; Parvez, K.; Feng, X.; Mullen, K. Graphene-based in-plane micro-supercapacitors with high power and energy densities. *Nat. Commun.* **2013**, *4*, 2487. [[CrossRef](#)] [[PubMed](#)]
72. Nagar, B.; Dubal, D.P.; Pires, L.; Merkoci, A.; Gomez-Romero, P. Design and fabrication of printed paper-based hybrid micro-supercapacitor by using graphene and redox-active electrolyte. *ChemSusChem* **2018**, *11*, 1849–1856. [[CrossRef](#)]
73. Oschatz, M.; Borchardt, L.; Pinkert, K.; Thieme, S.; Lohe, M.R.; Hoffmann, C.; Benusch, M.; Wisser, F.M.; Ziegler, C.; Giebel, L.; et al. Hierarchical carbide-derived carbon foams with advanced mesostructure as a versatile electrochemical energy-storage material. *Adv. Energy Mater.* **2014**, *4*, 1300645. [[CrossRef](#)]
74. Pinkert, K.; Oschatz, M.; Borchardt, L.; Klose, M.; Zier, M.; Nickel, W.; Giebel, L.; Oswald, S.; Kaskel, S.; Eckert, J. Role of surface functional groups in ordered mesoporous carbide-derived carbon/ionic liquid electrolyte double-layer capacitor interfaces. *ACS Appl. Mater. Interfaces* **2014**, *6*, 2922–2928. [[CrossRef](#)] [[PubMed](#)]
75. Huang, P.; Heon, M.; Pech, D.; Brunet, M.; Taberna, P.L.; Gogotsi, Y.S.; Lofland, J.D.; Simon, P. Micro-supercapacitors from carbide derived carbon (CDC) films on silicon chips. *J. Power Sources* **2013**, *225*, 240–244. [[CrossRef](#)]
76. Lu, Z.X.; Wang, N.N.; Zhang, Y.H.; Xue, P.; Guo, M.Q.; Tang, B.; Bai, Z.; Dou, S.X. Pyrite FeS₂@C nanorods as smart cathode for sodium ion battery with ultra-long lifespan and notable rate performance from tunable pseudocapacitance. *Electrochim. Acta* **2018**, *260*, 755–761. [[CrossRef](#)]
77. Chao, D.L.; Zhu, C.R.; Yang, P.H.; Xia, X.H.; Liu, J.L.; Wang, J.; Fan, X.F.; Savilov, S.V.; Lin, J.Y.; Fan, H.J.; et al. Array of Nanosheets render ultrafast and high-capacity Na-ion storage by tunable pseudocapacitance. *Nat. Commun.* **2016**, *7*, 12122–12130. [[CrossRef](#)] [[PubMed](#)]
78. Shabangoli, Y.; Rahmanifar, M.S.; Noori, A.; El-Kady, M.F.; Kaner, R.B.; Mousavi, M.F. Nile blue functionalized graphene aerogel as a pseudocapacitive negative electrode material across the full pH range. *ACS Nano* **2019**, *13*, 12567–12576. [[CrossRef](#)] [[PubMed](#)]
79. Raha, H.; Pradhan, D.; Guha, P.K. Structurally modified V₂O₅ based extrinsic pseudocapacitor. *Nanotechnology* **2022**, *33*, 255402. [[CrossRef](#)]
80. Rodrigues, M.A.; Catto, A.C.; Longo, E.; Nossol, E.; Lima, R.C. Characterization and electrochemical performance of CeO₂ and Eu-doped CeO₂ films as a manganese redox flow battery component. *J. Rare Earths* **2018**, *36*, 1074–1083. [[CrossRef](#)]
81. Brezesinski, T.; Wang, J.; Senter, R.; Brezesinski, K.; Dunn, B.; Tolbert, S.H. On the correlation between mechanical flexibility, nanoscale structure, and charge storage in periodic mesoporous CeO₂ thin films. *ACS Nano* **2010**, *4*, 967–977. [[CrossRef](#)] [[PubMed](#)]
82. Trasatti, S.; Buzzanca, G. Ruthenium dioxide: A new interesting electrode material. Solid state structure and electrochemical behaviour. *J. Electroanal. Chem. Interfacial Electrochem.* **1971**, *29*, A1–A5. [[CrossRef](#)]
83. Brousse, T.; Bélanger, D.; Long, J.W. To Be or Not To Be Pseudocapacitive? *J. Electrochem. Soc.* **2015**, *162*, A5185–A5189. [[CrossRef](#)]
84. Zhang, X.; Wang, M.; Zhu, G.; Li, D.; Yan, D.; Lu, T.; Pan, L. Porous cake-like TiO₂ derived from metal-organic frameworks as superior anode material for sodium ion batteries. *Ceram. Int.* **2017**, *43*, 2398–2402. [[CrossRef](#)]

85. Chen, R.; Yu, M.; Sahu, R.P.; Puri, I.K.; Zhitomirsky, I. The development of pseudocapacitor electrodes and devices with high active mass loading. *Adv. Energy Mater.* **2020**, *10*, 1903848. [[CrossRef](#)]
86. Kakaei, K.; Esrafil, M.D.; Ehsani, A. Graphene-based electrochemical supercapacitors. *Interface Sci. Technol.* **2019**, *27*, 339–386.
87. Chen, X.; Wu, Y.; Holze, R. Ag(e)ing and Degradation of Supercapacitors: Causes, Mechanisms, Models and Countermeasures. *Molecules* **2023**, *28*, 5028. [[CrossRef](#)] [[PubMed](#)]
88. Noori, A.; El-Kady, M.F.; Rahmanifar, M.S.; Kaner, R.B.; Mousavi, M.F. Towards establishing standard performance metrics for batteries, supercapacitors and beyond. *Chem. Soc. Rev.* **2019**, *48*, 1272–1341. [[CrossRef](#)]
89. Maria, F.R.; Raj, S.; Jaya, N.V.; Boopathi, G.; Kalpana, D.; Pandurangan, A. S-doped activated mesoporous carbon derived from the Borassus flabellifer flower as active electrodes for supercapacitors. *Mater. Chem. Phys.* **2019**, *240*, 122151. [[CrossRef](#)]
90. Choi, C.; Ashby, D.S.; Butts, D.M.; DeBlock, R.H.; Wei, Q.L.; Lau, J.; Dunn, B. Achieving high energy density and high power density with pseudocapacitive materials. *Nat. Rev. Mater.* **2020**, *5*, 5–19. [[CrossRef](#)]
91. Liu, H.; Liu, X.; Wang, S.; Liu, H.K.; Li, L. Transition metal based battery-type electrodes in hybrid supercapacitors: A review. *Energy Storage Mater.* **2020**, *28*, 122–145. [[CrossRef](#)]
92. Augustyn, V.; Come, J.; Lowe, M.A.; Kim, J.W.; Taberna, P.-L.; Tolbert, S.H.; Abruna, H.D.; Simon, P.; Dunn, B. High-rate electrochemical energy storage through Li^+ intercalation pseudocapacitance. *Nat. Mater.* **2013**, *12*, 518–522. [[CrossRef](#)] [[PubMed](#)]
93. Okubo, M.; Hosono, E.; Kim, J.; Enomoto, M.; Kojima, N.; Kudo, T.; Zhou, H.; Honma, I. Nanosize effect on high-rate Li-ion intercalation in LiCoO_2 electrode. *J. Am. Chem. Soc.* **2007**, *129*, 7444–7452. [[CrossRef](#)] [[PubMed](#)]
94. Brousse, T.; Toupin, M.; Dugas, R.; Athouël, L.; Crosnier, O.; Bélanger, D. Crystalline MnO_2 as possible alternatives to amorphous compounds in electrochemical supercapacitors. *J. Electrochem. Soc.* **2006**, *153*, A2171. [[CrossRef](#)]
95. Trasatti, S. Work function, electronegativity, and electrochemical behaviour of metals: III. Electrolytic hydrogen evolution in acid solutions. *J. Electroanal. Chem. Interfacial Electrochem.* **1971**, *39*, 163–184. [[CrossRef](#)]
96. Zhang, K.; Han, X.; Hu, Z.; Zhang, X.; Tao, Z.; Chen, J. Nanostructured Mn-based oxides for electrochemical energy storage and conversion. *Chem. Soc. Rev.* **2015**, *44*, 699–728. [[CrossRef](#)]
97. Tan, H.T.; Sun, W.; Wang, L.; Yan, Q. 2D transition metal oxides/hydroxides for energy-storage applications. *Chem. Nano. Mat.* **2016**, *2*, 562–577. [[CrossRef](#)]
98. Devaraj, S.; Munichandraiah, N. Effect of crystallographic structure of MnO_2 on its electrochemical capacitance properties. *J. Phys. Chem. C* **2008**, *112*, 4406–4417. [[CrossRef](#)]
99. Choi, C.; Kim, J.H.; Sim, H.J.; Di, J.; Baughman, R.H.; Kim, S.J. Microscopically buckled and macroscopically coiled fibers for ultra-stretchable supercapacitors. *Adv. Energy Mater.* **2017**, *7*, 1602021. [[CrossRef](#)]
100. Cao, L.; Zhu, J.; Li, Y.; Xiao, P.; Zhang, Y.; Zhang, S.; Yang, S. Ultrathin single-crystalline vanadium pentoxide nanoribbon constructed 3D networks for superior energy storage. *J. Mater. Chem. A* **2014**, *2*, 13136–13142. [[CrossRef](#)]
101. Ke, Q.; Guan, C.; Zhang, X.; Zheng, M.; Zhang, Y.W.; Cai, Y.; Zhang, H.; Wang, J. Surface-charge-mediated formation of $\text{H-TiO}_2@\text{Ni(OH)}_2$ heterostructures for high-performance supercapacitors. *Adv. Mater.* **2017**, *29*, 1604164. [[CrossRef](#)] [[PubMed](#)]
102. Yu, P.; Zhang, Z.; Zheng, L.; Teng, F.; Hu, L.; Fang, X. A novel sustainable flour derived hierarchical nitrogen-doped porous carbon/polyaniline electrode for advanced asymmetric supercapacitors. *Adv. Energy Mater.* **2016**, *6*, 1601111. [[CrossRef](#)]
103. Brezesinski, T.; Wang, J.; Tolbert, S.H.; Dunn, B. Ordered mesoporous $\alpha\text{-MoO}_3$ with iso-oriented nanocrystalline walls for thin-film pseudocapacitors. *Nat. Mater.* **2010**, *9*, 146–151. [[CrossRef](#)] [[PubMed](#)]
104. Mirzaei, M.; Abbas, Q.; Hunt, M.R.C.; Hall, P. Pseudocapacitive effect of carbons doped with different functional groups as electrode materials for electrochemical capacitors. *Energies* **2020**, *13*, 5577. [[CrossRef](#)]
105. Thomas, R.; Balachandran, M. Fuel coke derived nitrogen and phosphorus co-doped porous graphene structures for high-performance supercapacitors: The trail towards a brown-to-green transition. *J. Energy Storage* **2023**, *72*, 108799. [[CrossRef](#)]
106. Han, L.; Chen, X.; Zeng, S.; Liu, J.; Yang, Z.; Wang, Z.; Li, L.; Wang, H.; Hou, Z.; Xu, M. B, N dual doped coral-like carbon framework with superior pseudocapacitance and surface wettability. *Front. Mater.* **2021**, *8*, 705930. [[CrossRef](#)]
107. Razack, I.J.; Thomas, A.; Kota, S.; Varghese, M.; Chiriyankandath, J.S.; Nair, A.S. Graphene based materials for supercapacitors. *Mapana J. Sci.* **2020**, *19*, 87–137.
108. Mathew, E.E.; Balachandran, M. Role of defects in the band gap tailoring of carbon black. *Mapana J. Sci.* **2022**, *21*, 1–11.
109. Roduner, E. Size matters: Why nanomaterials are different? *Chem. Soc. Rev.* **2006**, *35*, 583–592. [[CrossRef](#)] [[PubMed](#)]
110. Pomerantseva, E.; Bonaccorso, F.; Feng, X.; Cui, Y.; Gogotsi, Y. Energy storage: The future enabled by nanomaterials. *Science* **2019**, *366*, eaan8285. [[CrossRef](#)]
111. Baig, N.; Kammakakam, I.; Falath, W. Nanomaterials: A review of synthesis methods, properties, recent progress, and challenges. *Mater. Adv.* **2021**, *2*, 1821–1871. [[CrossRef](#)]
112. Gogotsi, Y.; Penner, R.M. Energy storage in nanomaterials—capacitive, pseudocapacitive, or battery-like? *ACS Nano* **2018**, *12*, 2081–2083. [[CrossRef](#)] [[PubMed](#)]
113. Simon, P.; Gogotsi, Y.; Dunn, B. Where do batteries end and supercapacitors begin? *Science* **2014**, *343*, 1210–1211. [[CrossRef](#)] [[PubMed](#)]

114. Rauda, I.E.; Augustyn, V.; Saldarriaga-Lopez, L.C.; Chen, X.; Schelhas, L.T.; Rubloff, G.W.; Dunn, B.; Tolbert, S.H. Nanostructured pseudocapacitors based on atomic layer deposition of V_2O_5 onto conductive nanocrystal-based mesoporous ITO scaffolds. *Adv. Funct. Mater.* **2014**, *24*, 6717–6728. [[CrossRef](#)]
115. Sun, H.; Mei, L.; Liang, J.; Zhao, Z.; Lee, C.; Fei, H.; Ding, M.; Lau, J.; Li, M.; Wang, C.; et al. Three dimensional holey-graphene/nioobia composite architectures for ultrahigh-rate energy storage. *Science* **2017**, *356*, 599–604. [[CrossRef](#)]
116. Duan, H.-S.; Cook, J.B.; Tolbert, S.H.; Dunn, B. The development of pseudocapacitive properties in nanosized-MoO₂. *J. Electrochem. Soc.* **2015**, *162*, A5083–A5090.
117. Dunn, D.M. The proton diffusion coefficient for the nickel hydroxide electrode. *J. Electrochem. Soc.* **1970**, *117*, 729–732.
118. Wang, J.; Polleux, J.; Lim, J.; Dunn, B. Pseudocapacitive contributions to electrochemical energy storage in TiO₂ (anatase) nanoparticles. *J. Phys. Chem. C* **2007**, *111*, 14925–14931. [[CrossRef](#)]
119. Come, J.; Taberna, P.-L.; Hamelet, S.; Masquelier, C.; Simon, P. Electrochemical kinetic study of LiFePO₄ using cavity microelectrode. *J. Electrochem. Soc.* **2011**, *158*, A1090–A1093. [[CrossRef](#)]
120. Laskova, B.; Zukalova, M.; Zukal, A.; Bousa, M.; Kavan, L. Capacitive contribution to Li-storage in TiO₂ (B) and TiO₂ (anatase). *J. Power Sources* **2014**, *246*, 103–109. [[CrossRef](#)]
121. Zukalova, M.; Kalbac, M.; Kavan, L.; Exnar, I.; Graetzel, M. Pseudocapacitive lithium storage in TiO₂ (B). *Chem. Mater.* **2005**, *17*, 1248–1255. [[CrossRef](#)]
122. Tang, P.; Gao, P.; Cui, X.; Chen, Z.; Fu, Q.; Wang, Z.; Mo, Y.; Liu, H.; Xu, C.; Liu, J.; et al. Covalency competition induced active octahedral sites in spinel cobaltites for enhanced pseudocapacitive charge storage. *Adv. Energy Mater.* **2022**, *12*, 2102053. [[CrossRef](#)]
123. Passerini, M.; Liu, T.; Peng, N.; Zheng, R.; Cheng, X.; Zhu, H.; Yu, H.; Shui, M.; Shu, J. Lab-Scale in situ X-ray diffraction technique for different battery systems: Designs, applications, and perspectives. *Small Methods* **2019**, *3*, 1900119.
124. Liu, S.; Lin, H.; Song, Q.; Zhu, J.; Zhu, C. Anti-corrosion and reconstruction of surface crystal plane for Zn anodes by an advanced metal passivation technique. *Energy Environ. Mater.* **2023**, *6*, e12405. [[CrossRef](#)]
125. Liu, X.; Yin, L.; Ren, D.; Wang, L.; Ren, Y.; Xu, W.; Lapidus, S.; Wang, H.; He, X.; Chen, Z.; et al. In situ observation of thermal-driven degradation and safety concerns of lithiated graphite anode. *Nat. Commun.* **2021**, *12*, 4235. [[CrossRef](#)] [[PubMed](#)]
126. Tang, P.; Tan, W.; Deng, G.; Zhang, Y.; Xu, S.; Wang, Q.; Li, G.; Zhu, J.; Dou, Q.; Yan, X. Understanding pseudocapacitance mechanisms by synchrotron X-ray analytical techniques. *Energy Environ. Mater.* **2023**, *6*, e12619. [[CrossRef](#)]
127. Gao, P.; Tang, P.; Mo, Y.; Xiao, P.; Zhou, W.; Chen, S.; Dong, H.; Li, Z.; Xu, C.; Liu, J. Covalency competition induced selective bond breakage and surface reconstruction in manganese cobaltite towards enhanced electrochemical charge storage. *Green Energy Environ.* **2024**, *9*, 909–918. [[CrossRef](#)]
128. Medina-Carrasco, S.; Valverde, J.M. The calcium looping process for energy storage: Insights from in situ XRD analysis. *Chem. Eng. J.* **2022**, *429*, 132244. [[CrossRef](#)]
129. Guo, J.Z.; Wang, P.F.; Wu, X.L.; Zhang, X.H.; Yan, Q.; Chen, H.; Zhang, J.P.; Guo, Y.G. High-energy/power and low-temperature cathode for sodium-ion batteries: In situ XRD study and superior full-cell performance. *Adv. Mater.* **2017**, *29*, 1701968. [[CrossRef](#)] [[PubMed](#)]
130. Liu, B.T.W.; Ye, L.; Tsang, S.C.E. The contribution of synchrotron X-ray powder diffraction to modern zeolite applications: A mini-review and prospects. *Chem.* **2018**, *4*, 1778–1808.
131. Zhang, P.; Deng, X.; Li, W.; Ma, Z.; Wang, X. Electrochemical-induced surface reconstruction to NiFe-LDHs-based heterostructure as novel positive electrode for supercapacitors with enhanced performance in neutral electrolyte. *Chem. Eng. J.* **2022**, *449*, 137886. [[CrossRef](#)]
132. Kang, H.C.; Yan, H.; Winarski, R.P.; Holt, M.V.; Maser, J.; Liu, C.; Conley, R.; Vogt, S.; Macrander, A.T.; Stephenson, G.B. Focusing of hard x-rays to 16 nanometers with a multilayer Laue lens. *Appl. Phys. Lett.* **2008**, *92*, 221114. [[CrossRef](#)]
133. Liu, R.; Yang, L.; Wang, W.; Zhao, E.; Wang, B.; Zhang, X.; Liu, H.; Zeng, C. Surface redox pseudocapacitance-based vanadium nitride nanoparticles toward a long-cycling sodium-ion battery. *Mater. Today Energy* **2023**, *34*, 101300.
134. Wilkins, S.W.; Gureyev, T.E.; Gao, D.; Pogany, A.; Stevenson, A.W. Phase-contrast imaging using polychromatic hard X-rays. *Nature* **1996**, *384*, 335–338. [[CrossRef](#)]
135. Nugent, K.A.; Gureyev, T.E.; Cookson, D.F.; Paganin, D.; Barnea, Z. Quantitative phase imaging using hard X rays. *Phys. Rev. Lett.* **1996**, *77*, 2961–2964. [[CrossRef](#)]
136. Rehr, J.J.; Ankudinov, A.L. Progress in the theory and interpretation of XANES. *Coord. Chem. Rev.* **2005**, *249*, 131.
137. Ankudinov, C.; Chen, S.; Song, L. Tuning 2D MXenes by surface controlling and interlayer engineering: Methods, properties, and synchrotron radiation characterizations. *Adv. Funct. Mater.* **2020**, *30*, 2000869.
138. Babonneau, F.; Doeuff, S.; Leaustic, A.; Sanchez, C.; Cartier, C.; Verdaguer, M. XANES and EXAFS study of titanium alkoxides. *Inorg. Chem.* **1988**, *27*, 3166–3172.

139. Tanaka, I.; Mizoguchi, T.; Yamamoto, T. XANES and ELNES in ceramic science. *J. Am. Ceram. Soc.* **2005**, *88*, 2013–2029. [CrossRef]
140. Simon, P.; Gogotsi, Y. Capacitive energy storage in nanostructured carbon–electrolyte systems. *Acc. Chem. Res.* **2013**, *46*, 1094–1103. [CrossRef] [PubMed]
141. Liu, Y.; Liu, L.; Kang, L.; Ran, F. Energy storage mechanism of vanadium nitride via intercalating different atomic radius for expanding interplanar spacing. *Energy Environ. Mater.* **2022**, *5*, 565–571. [CrossRef]
142. Terban, M.W.; Billinge, S.J.L. Structural analysis of molecular materials using the pair distribution function. *Chem. Rev.* **2022**, *122*, 1208–1272. [CrossRef] [PubMed]
143. Banerjee, S.; Liu, C.-H.; Lee, J.D.; Kovayakh, A.V.; Koenigsman, G.O.; Prymak, C.; Liu, H.; Wang, L.; Abeykoon, A.M.M.; Wong, S.S.; et al. Improved models for metallic nanoparticle cores from atomic pair distribution function (PDF) analysis. *J. Phys. Chem. C* **2018**, *122*, 29498–29506. [CrossRef]
144. Petkov, V.; Billinge, S.J.L.; Larson, P.; Mahanti, S.D.; Vogt, T.; Rangan, K.K.; Kanatzidis, M.G. Structure of nanocrystalline materials using atomic pair distribution function analysis: Study of LiMoS₂. *Phys. Rev. B* **2002**, *65*, 092105. [CrossRef]
145. Zhan, C.; Lian, C.; Zhang, Y.; Thompson, M.W.; Xie, Y.; Wu, J.; Kent, P.R.C.; Cummings, P.T.; Jiang, D.; Wesolowski, D.J. Computational insights into materials and interfaces for capacitive energy storage. *Adv. Sci.* **2017**, *4*, 1700059. [CrossRef] [PubMed]
146. Chen, J.F.; Han, Y.L.; Kong, X.H.; Deng, X.Z.; Park, H.J.; Guo, Y.L.; Jin, S.; Qi, Z.K.; Lee, Z.; Qiao, Z.H.; et al. The origin of improved electrical double-layer capacitance by inclusion of topological defects and dopants in graphene for supercapacitors. *Angew. Chem. Int. Ed.* **2016**, *55*, 13822. [CrossRef] [PubMed]
147. Pak, A.J.; Paek, E.; Hwang, G.S. Tailoring the performance of graphene-based supercapacitors using topological defects: A theoretical assessment. *Carbon* **2014**, *68*, 734–741. [CrossRef]
148. Lukatskaya, M.R.; Dunn, B.; Gogotsi, Y. Multidimensional materials and device architectures for future hybrid energy storage. *Nat. Commun.* **2016**, *7*, 12647. [CrossRef]
149. Xue, C.; Zhang, Y.; Nie, Z.; Nie, C.; Zhang, J. High pseudocapacitive lithium-storage behaviors of amorphous titanium oxides with titanium vacancies and open channels. *Electrochim. Acta* **2023**, *444*, 142021. [CrossRef]
150. Zhao, Z.; Wu, Y.; Hu, R.; Lu, J.; Chen, D.; Li, T.; Guo, Y.; Zhang, L.; Chen, H.; Ye, Z.; et al. Intercalation pseudocapacitance in 2D VS₂/Ti₃C₂Tx MXene hybrids for all-climate and long-cycle sodium-ion batteries. *Adv. Funct. Mater.* **2023**, *33*, 2307794. [CrossRef]
151. Duan, H.; Du, L.; Zhang, S.; Chen, Z.; Wu, S. Superior lithium-storage properties derived from a high pseudocapacitance behavior for a peony-like holey Co₃O₄ anode. *J. Mater. Chem.* **2019**, *7*, 8327–8334. [CrossRef]
152. Zhang, Y.; Ma, Q.; Feng, K.; Guo, J.; Wei, X.; Shao, Y.; Zhuang, J.; Lin, T. Effects of microstructure and electrochemical properties of Ti/IrO₂-SnO₂-Ta₂O₅ as anodes on binder-free asymmetric supercapacitors with Ti/RuO₂-NiO as cathodes. *Ceram. Int.* **2020**, *46*, 17640–17650. [CrossRef]
153. Nguyen, T.; Montemor, M.F. Redox active materials for metal compound based hybrid electrochemical energy storage: A perspective view. *Appl. Surf. Sci.* **2017**, *422*, 492–497. [CrossRef]
154. Xu, L.; Cheng, C.; Yao, C.; Jin, X. Flexible supercapacitor electrode based on lignosulfonate-derived graphene quantum dots/graphene hydrogel. *Org. Electron.* **2020**, *78*, 105407. [CrossRef]
155. Casiraghi, C.; Hartschuh, A.; Lidorikis, E.; Qian, H.; Harutyunyan, H.; Gokus, T.; Novoselov, K.S.; Ferrari, A.C. Rayleigh imaging of graphene and graphene layers. *Nano Lett.* **2007**, *7*, 2711–2717. [CrossRef] [PubMed]
156. Hu, Z.; Zhu, Z.; Cheng, F.; Zhang, K.; Wang, J.; Chen, C.; Chen, J. Pyrite FeS₂ for high-rate and long-life rechargeable sodium batteries. *Energy Environ. Sci.* **2015**, *8*, 1309–1316. [CrossRef]
157. Mofarah, S.S.; Adabifiroozjae, E.; Yao, Y.; Koshy, P.; Lim, S.; Webster, R.; Liu, X.; Nekouei, R.K.; Cazorla, C.; Liu, Z.; et al. Protonassisted creation of controllable volumetric oxygen vacancies in ultrathin CeO_{2-x} for pseudocapacitive energy storage applications. *Nat. Commun.* **2019**, *10*, 2594. [CrossRef]
158. Kim, H.J.; Yeon, J.S.; Park, H.R.; Lee, S.J.; Kim, W.; Jang, G.; Jang, H.S. Intercalation pseudocapacitance of cation-exchanged molybdenum-based polyoxometalate for the fast and stable zinc ion storage. *ACS Appl. Mater. Interfaces* **2023**, *15*, 9350–9361. [CrossRef]
159. Xiu, Z.; Alfaruqi, M.H.; Gim, J.; Song, J.; Kim, S.; Thi, T.V.; Duong, P.T.; Baboo, J.P.; Mathew, V.; Kim, J. Hierarchical porous anatase TiO₂ derived from a titanium metal-organic framework as a superior anode material for lithium ion batteries. *Chem. Commun.* **2015**, *51*, 12274–12277. [CrossRef] [PubMed]
160. Cui, Y.; Chen, X.; Liang, J.; Liu, Z.; Yang, G.; Zhang, Q.; Fan, H.; Peng, F.; Duan, X. Boosting pseudocapacitive sodium storage while restraining the shuttle effect of polysulfides in holey nickel disulfide nanoplatelets by a polypyrrole-coating strategy. *Appl. Surf. Sci.* **2024**, *669*, 160524. [CrossRef]
161. Hao, B.; Yan, Y.; Wang, X.; Chen, G. Synthesis of anatase TiO₂ nanosheets with enhanced pseudocapacitive contribution for fast lithium storage. *ACS Appl. Mater. Interfaces* **2013**, *5*, 6285–6291. [CrossRef] [PubMed]

162. Wu, D.; Kang, Y.; Wang, F.; Yang, J.; Xu, Y.; Zhuang, Y.; Wu, J.; Zeng, J.; Yang, Y.; Zhao, J. Surface-redox pseudocapacitance-dominated charge storage mechanism enabled by the reconstructed cathode/electrolyte interface for high-rate magnesium batteries. *Adv. Energy Mater.* **2023**, *13*, 2301145. [[CrossRef](#)]
163. Kim, H.-S.; Cook, J.B.; Lin, H.; Ko, J.S.; Tolbert, S.H.; Ozolinsand, V.; Dunn, B. Oxygen vacancies enhance pseudocapacitive charge storage properties of MoO_{3-x} . *Nat. Mater.* **2017**, *16*, 454–460. [[CrossRef](#)] [[PubMed](#)]
164. Yang, H.; Wang, D.; Liu, Y.L.; Liu, Y.H.; Zhong, B.; Song, Y.; Kong, Q.; Wu, Z.; Guo, X. Improvement of cycle life for layered oxide cathodes in sodium-ion batteries. *Energy Environ. Sci.* **2024**, *17*, 1756–1780.
165. Cai, Y.; Chu, R.; Huang, S.; Ren, H.; Srinivasan, M. Amorphous manganese dioxide with the enhanced pseudocapacitive performance for aqueous rechargeable zinc-ion battery. *Chem. Eng. J.* **2020**, *396*, 125221. [[CrossRef](#)]
166. Zhang, L.; Miao, L.; Zhang, B.; Wang, J.; Liu, J.; Liu, Q.; Wan, H.; Jiang, J. A durable $\text{VO}_2(\text{M})/\text{Zn}$ battery with ultrahigh rate capability enabled by pseudocapacitive proton insertion. *J. Mater. Chem. A* **2020**, *8*, 1731–1740. [[CrossRef](#)]
167. Avvaru, V.S.; Vincent, M.; Fernandez, I.J.; Hinder, S.J.; Etacheri, V. Unusual pseudocapacitive lithium-ion storage on defective Co_3O_4 nanosheets. *Nanotechnology* **2022**, *33*, 225403. [[CrossRef](#)]
168. Xu, J.; Liu, Z.; Wang, Q.; Li, J.; Huang, Y.; Wang, M.; Cao, L.; Yao, W.; Wu, H.; Chen, C. Facile tailoring of surface terminations of MXenes by doping Nb element: Toward extraordinary pseudocapacitance performance. *ACS Appl. Mater. Interfaces* **2023**, *15*, 15367–15376. [[CrossRef](#)] [[PubMed](#)]
169. Yao, J.; Li, F.; Zhou, R.; Guo, C.; Liu, X.; Zhu, Y. Phosphorous-doped carbon nanotube/reduced graphene oxide aerogel cathode enabled by pseudocapacitance for high energy and powerzinc-ion hybrid capacitors. *Chin. Chem. Let.* **2024**, *35*, 108354. [[CrossRef](#)]
170. Ding, J.; Huang, Y.; Cheng, W.; Sheng, R.; Liu, Z.; Wang, X.; Guo, Y.; Wang, J.; Jia, D.; Tang, X.; et al. Boosting ion diffusion kinetics of $\text{Fe}_2\text{O}_3/\text{MoC@NG}$ via heterointerface engineering and pseudocapacitance behavior: An alternative high-rate anode for high-capacity lithium dual-ion batteries. *Chem. Eng. J.* **2024**, *481*, 148499. [[CrossRef](#)]
171. Pang, X.; Ji, S.; Zhang, P.; Feng, W.; Zhang, L.; Li, K.; Tang, Y.; Liu, Y. Interlayer doping of pseudocapacitive hydrated vanadium oxide via Mn^{2+} for high-performance aqueous zinc-ion battery. *Electrochim. Acta* **2023**, *441*, 141810. [[CrossRef](#)]
172. Mitchell, J.B.; Lo, W.C.; Genc, A.; LeBeau, J.; Augustyn, V. Transition from battery to pseudocapacitor behavior via structural water in tungsten oxide. *Chem. Mater.* **2017**, *29*, 3928–3937. [[CrossRef](#)]
173. El-Kady, M.F.; Strong, V.; Dubin, S.; Kaner, R.B. Laser scribing of high-performance and flexible graphene-based electrochemical capacitors. *Science* **2012**, *335*, 1326–1330. [[CrossRef](#)] [[PubMed](#)]
174. Xu, Y.; Lin, Z.; Huang, X.; Liu, Y.; Huang, Y.; Duan, X. Flexible Solid-State Supercapacitors Based on Three-Dimensional Graphene Hydrogel Films. *ACS Nano* **2013**, *7*, 4042–4049. [[CrossRef](#)] [[PubMed](#)]
175. Zou, K.Y.; Deng, W.T.; Silvester, D.S.; Zou, G.Q.; Hou, H.S.; Banks, C.E.; Li, L.J.; Hu, J.G.; Ji, X.B. Carbonyl chemistry for advanced electrochemical energy storage systems. *ACS Nano* **2024**, *18*, 19950–20000. [[CrossRef](#)]
176. Xu, H.-H.; Yue, L.; Tang, T.; Liu, F.; Zhu, H.-J.; Bao, S.-J. Preparation of chitosan and citric acid crosslinked membrane and its application in quasi-solid supercapacitors. *Rare Met.* **2023**, *42*, 430–437. [[CrossRef](#)]
177. Xie, J.; Sun, X.; Zhang, N.; Xu, K.; Zhou, M.; Xie, Y. Layer-by-layer $\beta\text{-Ni(OH)}_2$ /graphene nanohybrids for ultraflexible all-solid-state thin-film supercapacitors with high electrochemical performance. *Nano Energy* **2013**, *2*, 65–74. [[CrossRef](#)]
178. Meng, C.; Liu, C.; Chen, L.; Hu, C.; Fan, S. Highly flexible and all-solid-state paperlike polymer supercapacitors. *Nano Lett.* **2010**, *10*, 4025–4031. [[CrossRef](#)]
179. Dubal, D.P.; Holze, R. Synthesis, properties, and performance of nanostructured metal oxides for supercapacitors. *Pure Appl. Chem.* **2014**, *86*, 611. [[CrossRef](#)]
180. Peng, L.; Peng, X.; Liu, B.; Wu, C.; Xie, Y.; Yu, G. Ultrathin Two-dimensional MnO_2 /graphene hybrid nanostructures for high-performance, flexible planar supercapacitors. *Nano Lett.* **2013**, *13*, 2151–2157. [[CrossRef](#)]
181. He, Y.; Chen, W.; Li, X.; Zhang, Z.; Fu, J.; Zhao, C.; Xie, E. Freestanding three-dimensional graphene/ MnO_2 composite networks as ultralight and flexible supercapacitor electrodes. *ACS Nano* **2013**, *7*, 174–182. [[CrossRef](#)]
182. Choi, B.G.; Chang, S.-J.; Kang, H.-W.; Park, C.P.; Kim, H.J.; Hong, W.H.; Lee, S.; Huh, Y.S. High performance of a solid-state flexible asymmetric supercapacitor based on graphene films. *Nanoscale* **2012**, *4*, 4983–4988. [[CrossRef](#)] [[PubMed](#)]
183. Hu, Y.; Guan, C.; Feng, G.; Ke, Q.; Huang, X.; Wang, J. Flexible asymmetric supercapacitor based on structure-optimized Mn_3O_4 /reduced graphene oxide nanohybrid paper with high energy and power density. *Adv. Funct. Mater.* **2015**, *25*, 7291–7299. [[CrossRef](#)]
184. Bo, L.W.; Hu, L.; Wang, N.Z.; Sun, M.X.; Ren, X.H.; Li, Z.J.; Yao, X.J.; Jia, C.Y. Methylene blue modified graphene film as high-performance electrode towards all-in-one flexible supercapacitors with “all-graphene” structure. *J. Power Sources* **2024**, *591*, 233839. [[CrossRef](#)]
185. Long, J.W.; Han, T.L.; Zeng, X.B.; Chen, C.B.; Zhan, P.; Zhang, H.G.; Liu, J.Y. Rationally engineering a quasi-solid-state flexible self-healing secondary battery using hydrogel-based water-in-salt electrolyte and electrochemically deposited electrodes. *Nano Lett.* **2024**, *24*, 11429–11437. [[CrossRef](#)]

186. Kumar, R.; Ranjan, B.; Kaur, D. Pseudocapacitive performance of reactively co-sputtered titanium chromium nitride nanopyramids towards flexible supercapacitor with Li-ion storage. *J. Energy Storage* **2024**, *84*, 110866. [[CrossRef](#)]
187. Zong, Y.; Chen, H.; Wang, J.; Wu, M.; Chen, Y.; Wang, L.; Huang, X.; He, H.; Ning, X.; Bai, Z.; et al. Cation defect-engineered boost fast kinetics of two-dimensional topological Bi_2Se_3 cathode for high-performance aqueous Zn-ion batteries. *Adv. Mater.* **2023**, *35*, 2306269. [[CrossRef](#)]

Disclaimer/Publisher's Note: The statements, opinions and data contained in all publications are solely those of the individual author(s) and contributor(s) and not of MDPI and/or the editor(s). MDPI and/or the editor(s) disclaim responsibility for any injury to people or property resulting from any ideas, methods, instructions or products referred to in the content.